MASTERARBEIT | MASTER'S THESIS

Titel | Title

The Role of Ploidy in the Evolution of Complex Karyotype Formation

verfasst von | submitted by

Ana Markovic BSc

angestrebter akademischer Grad | in partial fulfilment of the requirements for the degree of

Master of Science (MSc)

Wien | Vienna, 2024

Studienkennzahl lt. Studienblatt | Degree programme code as it appears on the student record sheet:	UA 066 865
Studienrichtung lt. Studienblatt | Degree programme as it appears on the student record sheet:	Masterstudium Molecular Biology
Betreut von | Supervisor:	Assoz. Prof. Christopher Campbell PhD

Acknowledgments

I want to thank Assoc.-Prof. Christopher Campbell, PhD, and Manuel Alonso Y Adell, PhD, for the opportunity to work on this research project. Their expertise and guidance have been essential in my development throughout my master's journey.

I also want to extend my gratitude to Tamara Klockner, PhD, for her constant encouragement and kindness.

I am very grateful to all my colleagues for being supportive and helpful during the entire project.

Additionally, I would like to thank Sophie for her enthusiasm and support, which greatly enhanced my lab experience.

I want to thank my family and friends for their unwavering support, patience, and belief in me. I especially want to thank my mom for always encouraging me and patiently handling all my blockades.

Also, a huge thank you goes to Nikoleta, who has been by my side throughout this journey, providing unconditional support and friendship when I needed it most.

For Andrija.

Thank you!

Table of content

1. Introduction

1.1 Correct vs erroneous chromosome segregation

Accurate chromosome segregation is a fundamental process in the life of all dividing cells. It is carefully orchestrated by various mechanisms that give rise to two healthy daughter cells. A dividing cell enters mitosis with replicated genetic material, which is condensed into chromosomes. In parallel, centrosomes, protein structures that facilitate mitotic spindle formation, are also duplicated and move toward opposite poles of the cell. Thread-like protein structures called microtubules (MTs) are organized by the mitotic spindle, and together with different motor proteins, they position each chromosome in the middle of the mitotic cell, forming a metaphase plate. Each chromosome contains a kinetochore (KT), a protein structure formed on the centromeric DNA, which serves as a 'docking station' for microtubules (this interaction is called KT-MT attachment) (Cheeseman, 2014). During metaphase, the cell must ensure that each chromosome is attached to the microtubules originating from both poles (bi-oriented attachments). This delicate process involves multiple trial-and-error steps, ensuring the cell divides chromosomes only after all correct attachments are established **(Figure 1a)** (Tanaka, 2005).

Unresolved KT-MT attachment errors can lead to whole-chromosome missegregation. For example, when a chromosome is attached to the microtubules that come from only one of the poles (syntelic attachment), sister chromatids will not segregate, but the whole chromosome will be pulled only to one pole (chromosome non-disjunction). Another example of chromosome missegregation is lagging chromosome. This phenomenon occurs when one kinetochore (from one sister chromatid) is attached to microtubules coming from both poles, causing it to remain in the metaphase plate even after the cell enters anaphase (Baudoin & Bloomfield, 2021) **(Figure 1b, left).** Additionally, chromosome missegregation can be a consequence of unresolved DNA damage that occurred earlier in the cell cycle, and it could lead to chromosome breakage, which results in so-called focal changes in chromosome numbers or end-to-end chromosome fusions (chromosome bridge formation) (Ichijima et al., 2010; Umbreit et al., 2020) **(Figure 1b, left)**. Although rare (~1 per 100 cell divisions), all these examples of abnormal

chromosome segregation can lead to numerical (whole chr. and chr. arms) and structural (small chr. regions = focal changes) karyotype changes – aneuploidy (Burrell et al., 2013; Tijhuis et al., 2019).

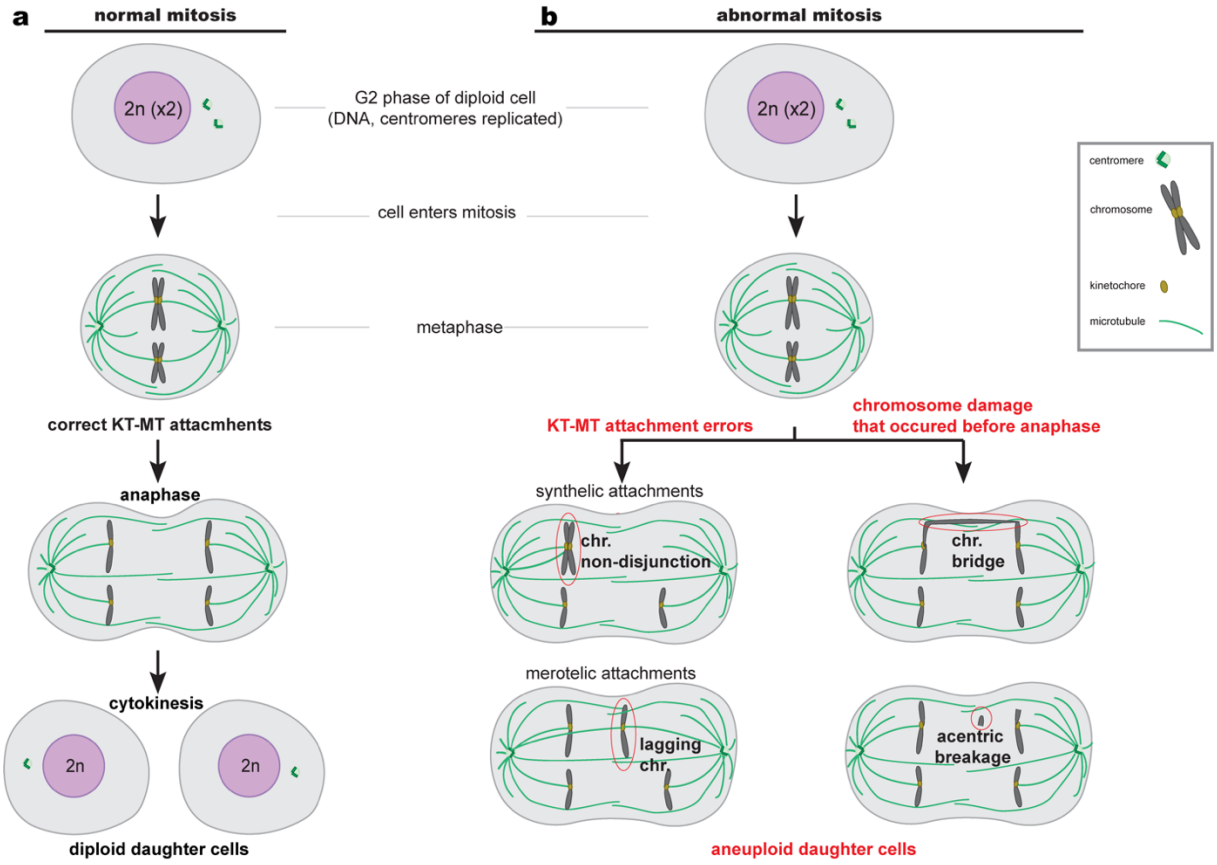

Figure 1: Normal mitosis vs aneuploidy. a) normal mitosis leads to two identical daughter cells forming from a single diploid cell. b) abnormal mitosis leads to aneuploid daughter cells and can be caused by multiple unresolved errors. (left) Kinetochore-microtubule (KT-MT) attachment errors can lead to chromosome non-disjunction and lagging chromosomes. These types of errors occur during the metaphase-to-anaphase transition. (right) Additionally, if chromosome damage is not accurately repaired, it can lead to chromosome bridge formation or acentric chromosome breakage during anaphase, resulting in chromosome missegregation and aneuploidy. The figure was adapted from (Baudoin & Bloomfield, 2021).

1.2 Chromosomal instability (CIN) and aneuploidy

When the above-mentioned chromosome missegregation events occur at high rates and lead to a deviation from a balanced complement of chromosomes in daughter cells, this is defined as chromosomal instability (CIN). When some karyotype deviations persist, the cell is defined as aneuploid. As mentioned above, the term aneuploidy describes changes in the number of whole chromosomes or chromosome arms. In other words, aneuploidy is a consequence of CIN (Ben-David & Amon, 2020; Sansregret et al., 2018). Once acquired, aneuploidy itself can induce further chromosomal instabilities; it has been shown that even single chromosome aneuploidies can lead to increased pre-mitotic DNA errors, which can lead to CIN (Passerini et al., 2016; Santaguida et al., 2017).

Aneuploidy affects various cellular processes, as shown in yeast and mammalian cells. This includes disruption in gene expression, protein synthesis, and cell signaling pathways (Beach et al., 2017; Schukken & Sheltzer, 2022). Aneuploidy can interfere with cell cycle regulation, leading to uncontrolled proliferation or cell death (Santaguida et al., 2017; Stingele et al., 2012; Torres et al., 2007). Furthermore, it can create cellular stress, triggering stress response pathways and increasing oxidative damage and metabolic dysregulation (Oromendia et al., 2012; Williams et al., 2008).

Considering all its adverse effects, aneuploidy is highly detrimental (Santaguida & Amon, 2015) and has a significant impact on both somatic and germline cells. Germline aneuploidy directly accounts for infertility, pregnancy loss, and developmental disorders, resulting in only a small proportion of aneuploid live births, such as trisomy 21 (Down syndrome) (Cohen, 2002; Hassold & Hunt, 2001; Wartosch et al., 2021). On the other hand, somatic cell aneuploidy is implicated in tumorigenesis, genomic instability, tumor evolution, metastasis, drug resistance, and reduced cancer patient survival. With 90% of solid tumors and 50% of hematopoietic tumors having some degree of aneuploidy, along with CIN, aneuploidy is one of the hallmarks of cancer (Andrade et al., 2023; Bakhoum et al., 2018; Hassold & Hunt, 2001; Ippolito et al., 2021; Lee et al., 2011; Lukow et al., 2021; van Dijk et al., 2021). This association between aneuploidy and tumor progression,

despite its detrimental effects on cellular fitness, is known as the “aneuploidy paradox” (Sheltzer & Amon, 2011; Weaver & Cleveland, 2008).

In the context of tumor evolution, aneuploidy and CIN develop and maintain genetic heterogeneity within a tumor, resulting in a population of cells with unique phenotypic and functional characteristics – intratumor diversity (Andrade et al., 2023; Vendramin et al., 2021). This heterogeneity allows for the selection of subclones that are better equipped to survive and proliferate under various stress sources, such as those imposed by chemotherapy or targeted therapies, accelerating tumor progression (Andrade et al., 2023; Burkard & Weaver, 2017; Burrell et al., 2013; Devon A. Lukow1, 2022; Laughney et al., 2015; Lee et al., 2011).

1.3 Mitotic errors and Spindle Assembly Checkpoint (SAC) function

As mentioned in **1.1**, aneuploidy can result from various defects in chromosome segregation and cell division processes. However, the cell has a surveillance mechanism called the Spindle Assembly Checkpoint (SAC) that prevents cell progression to anaphase until all chromosomes establish correct and stable KT-MT attachments (bioriented) (see **1.1**) (Tanaka, 2005), ensuring faithful division.

As shown in the simplified graph in **Figure 2,** SAC is a multi-step mechanism. Errors in KT-MT attachments are sensed by Mps1, protein kinase, which phosphorylates the outer kinetochore protein KNL1, leading to the formation of mitotic checkpoint complex (MCC), a tetrameric complex comprised of Mad2, Bub3, BubR1, and Cdc20 (McAinsh & Kops, 2023). MCC binds to and inhibits the activity of the Anaphase Promoting Complex/Cyclosome (APC/C), a key regulator of sister chromatid separation.

The APC/C is a multi-subunit E3 ubiquitin ligase that orchestrates the metaphase-to-anaphase transition in the mitotic cell. One of the essential cell cycle regulators, Cdc20, plays an important role in both SAC and APC/C activity (Zhang et al., 2024). When Cdc20 binds to APC/C, it activates it and allows it to degrade securin and cyclin B. Once

degraded, securin releases separase, an enzyme that will cleave components of the cohesin complex that holds sister chromatids together. As a result, sister chromatids will be physically separated upon APC/C activation. On the other hand, the degradation of cyclin B1 triggers the destruction of other regulators of mitosis, such as Cdc20. Now, APC/C will bind to another cell cycle regulator, Cdh1, which will remain active from the anaphase onset throughout G1 to ensure proper division and growth of the newly formed daughter cells (Schrock et al., 2020).

Inhibition of APC/C by MCC allows cyclin B and securin to remain intact and prevent anaphase onset, giving the cell enough time to correct KT-MT attachment errors. Once all kinetochores are stably attached to microtubules, the SAC is silenced, leading to the disassembly of the MCC and the release of APC/C, allowing for the completion of mitosis (Lara-Gonzalez et al., 2021; Maiato & Silva, 2023; Mora-Bermudez et al., 2022; Schrock et al., 2020).

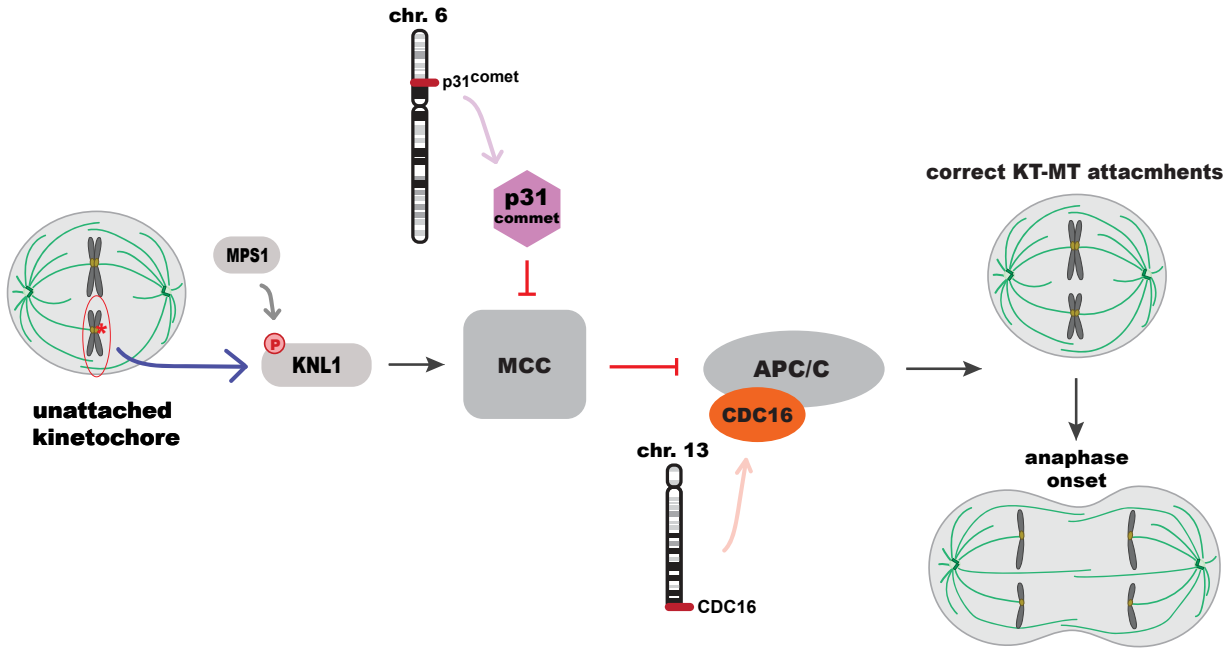

Figure 2: Mitotic errors and SAC function. Simplified graphic of the spindle assembly checkpoint (SAC) function in assuring correct chromosome segregation in mitosis. When kinetochore-microtube (KT-MT) attachments in metaphase-chromosome are not properly established, this triggers phosphorylation of the outer kinetochore protein KNL1, leading to mitotic checkpoint (MCC) activation. When active, the MCC inhibits the anaphase promoting complex/cyclosome (APC/C), giving the cell more time to fix the attachment errors. Once the KT-MT attachments are corrected, MCC production stops, allowing APC/C activity, which leads to anaphase. Two highlighted proteins in this graphic are p31commet and CDC16. p31commet plays a role in MCC disassembly, while CDC16 is a part of APC/C; therefore, both proteins promote the onset of anaphase.

1.4 Polyploidy

Another phenomenon that significantly contributes to cancer evolution is whole genome duplication (WGD). WGD leads to the duplication of the entire genome of the cell, giving rise to tetraploid cells (having four copies of each chromosome). If WGD is unregulated and occurs as a mistake in cell division, it can lead to genomically unstable, aneuploid, and tumorigenic cells. Having greater karyotypic complexity, these polyploid cells can exhibit strong functional heterogeneity with a plethora of evolutionary possibilities (Baudoin & Bloomfield, 2021; Bielski et al., 2018; Fujiwara et al., 2005). This makes WGD one of the hallmarks of cancer, occurring in more than 30% of cancers (Quinton et al., 2021; Zack et al., 2013). In this report, I will assess the differences regarding aneuploidy in the polyploid background of two human cell lines to understand the modes of karyotype evolution in vitro.

1.4.1 Whole genome doubling (WGD) in nature and cancer: *Mechanisms and consequences*

Polyploidy, specifically whole genome doubling (WGD), has contrasting roles in normal development and cancer. Typically, proliferating somatic cells are diploid (2n) and maintain that state through highly regulated processes (Lens & Medema, 2019; Maiato & Silva, 2023; McAinsh & Kops, 2023), some of which are mentioned in the chapters above.

Therefore, WGD is a relatively rare event in healthy tissues, but it is confirmed across different mammalian species in the following tissues: liver, heart, pancreas, bone marrow, and breast (Peterson & Fox, 2021).

Multiple regulated mechanisms evolved to give rise to WGD cells: endoreduplication, endomitosis, cytokinesis failure, and cell fusion. When it occurs in healthy tissues, WGD is highly regulated, providing cells with certain advantages needed in specific tissues (Vittoria et al., 2023). For example, polyploidy is commonly seen in megakaryocytes, the cells responsible for platelet production. As they differentiate, megakaryocytes switch from normal mitosis to endomitosis, a form of polyploidization, where the cell goes through mitosis but skips cytokinesis, which results in a daughter cell with a duplicated genome **(Figure 3)**. In megakaryocyte, endomitosis can happen more than once, giving rise to giant polyploid megakaryocyte (16n to 128n) that are more fit for efficient platelet production (Donne et al., 2020; Mazzi et al., 2018). Cell fusion leads to the formation of osteoclasts, multinucleated cells derived from the fusion of monocyte/macrophage precursors. These polyploid osteoclasts are more efficient in bone resorption, playing a pivotal role in skeletal development and bone mass regulation (Teitelbaum, 2000). Also, the adult liver consists of ~ 50% polyploid hepatocytes that play essential roles in normal homeostasis and regeneration (Donne et al., 2020). Polyploidization of hepatocytes predominantly occurs via cytokinesis failure (Duncan, 2013) and appears to be tumor-protective, potentially reflecting an evolutionary adaptation that enhances hepatocyte resilience to toxic challenges (Zhang et al., 2018).

If any of these polyploidization mechanism occur in an uncontrolled manner, they can give rise to malignancy. Proliferating polyploid cells experience higher rates of chromosome-missegregation/chromosomal instability (CIN), which results in high karyotype abnormalities. The increased genomic instability fuels tumor evolution, generating significant intratumoral heterogeneity. Finally, this heterogeneity can lead to the selection of subclones that are better adapted to survive and proliferate, potentially displaying increased resistance to therapies (Ganem et al., 2007; Vittoria et al., 2023). This was first demonstrated in a 2005 publication by Fujiwara et al., where they showed that polyploid (WGD+) mouse mammary epithelial p53 null cells are prone to

chromosome missegregations and are sufficient for tumor formation when injected into nude mice, unlike their diploid counterparts. These WGD+ cells were generated by inhibiting cytokinesis (Fujiwara et al., 2005). Further studies also point out the oncogenic potential of WGD+ cells, independent of the mechanisms behind polyploidization of these cells, as seen in virus-induced fusion of diploid human fibroblasts (Duelli et al., 2007); overexpression of Aurora B leads to premature chromatid separation, or endomitosis that results in tetraploidization (Nguyen et al., 2009); telomere dysfunction of DNA damage that causes endoreduplication and mitotic failure will lead to oncogenic WGD+ cells (Davoli & de Lange, 2012).

In summary, whole genome duplication (WGD) is one of the most prevalent genetic changes observed in human cancer (seen in 30-40% of all solid cancers) (Bielski et al., 2018; Lopez et al., 2020; Quinton et al., 2021; Zack et al., 2013).

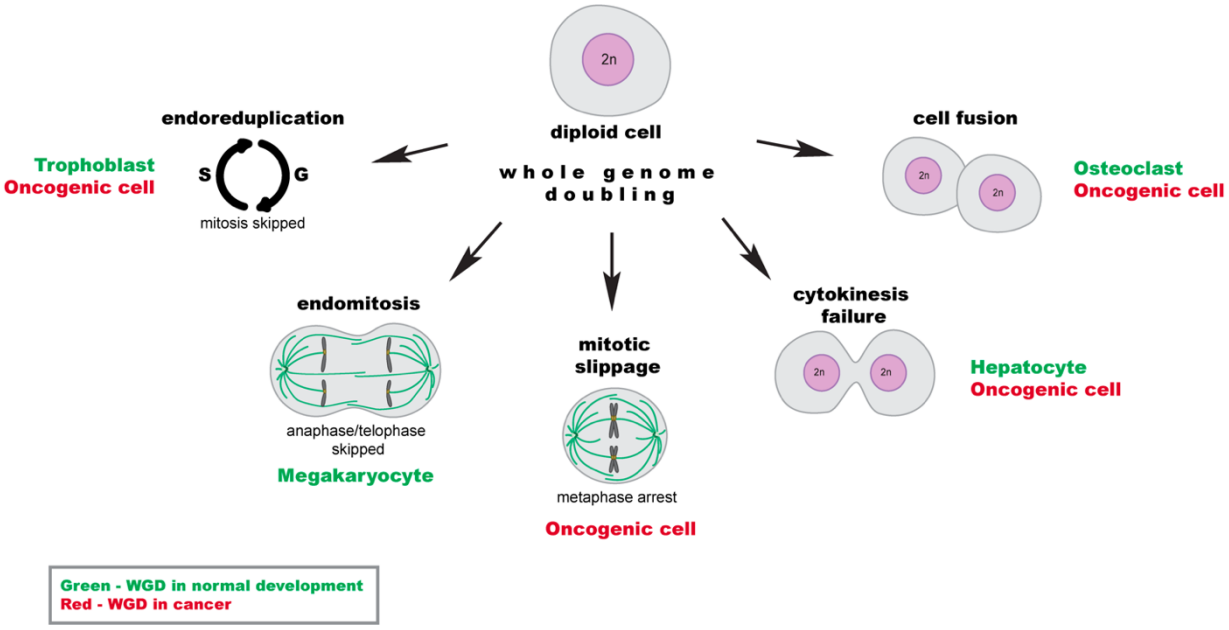

Figure 3: Mechanisms of Whole Genome Doubling (WGD). Multiple molecular mechanisms can lead to a whole genome doubling in normal development and cancer. Endoreduplication occurs when a cell skips mitosis and cytokinesis (typical in trophoblasts). Endomitosis and mitotic slippage occur when the cell enters mitosis but becomes arrested due to the activation of the spindle assembly checkpoint (SAC); because of this arrest, the cell cannot segregate chromosomes (typical in megakaryocytes). Cytokinesis failure is a result of incomplete contractile ring formation at the mid-body of the dividing cell (typical in hepatocytes). Cell fusion is typical in osteoclasts and can also be induced by viruses.

1.5 Aneuploidy patterns in diploid vs tetraploid cells

As pointed out above, aneuploid cells often experience various fitness defects and often die due to competition with normal neighboring cells. However, when a few resilient aneuploid cells survive and proliferate at normal rates, they typically exhibit higher stress resistance, making them more competitive in the tumor microenvironment, which may contribute to the frequent progression of malignancies after treatment (Vitale et al., 2011; Wang & Tamori, 2024). Aneuploidy patterns and frequencies vary across different cancer types (Beroukhim et al., 2010; Zack et al., 2013). Some aneuploidies are frequently found in various cancer types, such as gains of chromosome arms 8q and 20q. On the other hand, some aneuploidies are cancer-type-specific, such as chromosome 7 gain and chromosome 10 loss in glioblastoma (Bigner et al., 1990) or loss of 3p arm squamous cancers (Baker, Waise, et al., 2024). Considering whole genome doubling, the aneuploidy landscape changes compared to diploid cancer cells. Analysis of WGD+ vs WGD- subclones, the number of copy number alterations (CNAs) is greater in WGD+, which is in line with higher rates of CIN that is characteristic for WGD+ cells (Baker, Lai, et al., 2024; Watkins et al., 2020). WGD+ cells can also tolerate aneuploidies better, which allows for the formation of very complex karyotypes (Dewhurst et al., 2014). When comparing aneuploidy landscapes of chromosome gains, for the most part, they are similar in WGD+ and WGD- cells (Baker, Lai, et al., 2024; Prasad et al., 2022). However, WGD highly influences the frequency of chromosome loss occurrences. In a diploid background, losses of chromosome arms that carry many essential genes were negatively selected, which is not the case in WGD+ cells (Lopez et al., 2020). In line with

this, WGD+ tumors have an average number of 3 copies of each chromosome (Bielski et al., 2018).

In general, the rise in genomic instability likely allows WGD tumors to exhibit greater adaptability to therapy, which contributes to their poor prognosis (Baker, Waise, et al., 2024).

1.6 Aims of this study

To investigate the influence of ploidy on the development and composition of optimized complex karyotypes, *Manuel Alonso Adell* used two different p53-deleted human cell lines with varying ploidy states. He exposed them to an inhibitor of spindle assembly checkpoint kinase MPS1 (reversine) for 90 days. For this, Adell used the same adaptation protocol as in their recent publication (Adell et al., 2023), where he adapted multiple populations (~24) of each cell line to high rates of CIN. This adaptation protocol allowed him to track karyotypic changes that occur over time and to observe an active selection of specific aneuploidies that made cells more fit to survive long-term reversine treatment (see **Figure 8**). It is important to note that each cell line used in this report is p53 null since this allows cells to propagate even though they are exposed to continuous chromosome missegregation.

In their paper, *Adell & Klockner et al.* identified differences and similarities in complex karyotype pattern formation among different adapted cell lines of diploid background. They observed “uniformity” of aneuploidy patterns among all populations of the same cell line by the end of adaptation to CIN (after 90 days). Loss of chromosome 13q in adapted diploid HAP1 and loss of chromosome 6p in adapted diploid RPE1 cell lines were present in each population of the respective cell lines. When correlating the growth fitness of these adapted populations with the presence of 13q or 6p losses, they found that cells that lost their respective chromosome by day 60 were significantly more fit to survive further CIN induction. Further investigation, which involved introducing chromosome 13q and 6p losses in non-adapted dipHAP1 cells using CRISPR-Cas9, led to the discovery of two

genes (found on these chromosomes) that play an active role in the spindle assembly checkpoint, see **Figure 2.**

Similarly, in this report, I will first analyze adaptation to SAC inhibition in haploid, diploid, and tetraploid cells. To do this, I will analyze the NGS sequencing data alongside growth data from five cell lines that *A. Adell* previously used for long-term SAC inhibition adaptation protocol. The five cell lines include: *myeloid leukemia*: haploid HAP1; diploid HAP1; tetraploid HAP1; and e*pithelial noncancer*: diploid RPE1 and tetraploid RPE1. Cells originating from the same source (myeloid or epithelial) exhibit identical chromosome ratios at the population level, differing only in total DNA content (haploid, diploid, or tetraploid). As in their publication, here, twenty-four cell lines of each ploidy were previously subjected to reversine and sequenced to determine their chromosome copy numbers. Additionally, six cell lines of each ploidy will undergo parallel adaptation without reversine to assess the stability of polyploid cell karyotypes over time. A colony formation assay was used to measure growth rates of adapted cell lines (reversine treated) vs non-adapted (grown under standard conditions). We used these cell lines to address how the ploidy state influences the aneuploidy patterns that arise over time due to high rates of chromosomal instability (CIN).

I hypothesize that increased ploidy will result in a broader range of potentially beneficial aneuploidies, but the impact of individual aneuploidies will be diminished. To test this hypothesis, I plan to delete one copy of chromosomes 13q and 6p in tetraploid HAP1 cells and compare the effects on growth with and without reversine to diploid HAP1 cell lines with engineered chromosome loss from published data.

In Summary, I want to determine the effect of ploidy on complex karyotype patterns that emerge over time in human cell lines and the effect of engineered chromosome losses in diploid vs. tetraploid backgrounds.

2. Materials and Methods

2.1 Cell lines and cell culture

All cell lines were p53 null mutants previously engineered by Manuel Y Adell Alonso (Adell & Klockner, 2023). The Diploid HAP1 cell line was derived from single-cell sorting for a stable diploid clone from a haploid parental population. Tetraploid cell lines were obtained from tetraploidization of diploid p53 null cell lines. Information about their tissue types, phenotype, and culture conditions are highlighted in Supplemental Table 1. Depending on the cell type, cell lines were cultured in respective media. A humidified growth chamber was used at 37°C and 5 % CO_2 for all the cell lines.

2.1.1 Reversine treatment in different experimental set-ups

The above-described cell lines (five cell lines, three ploidy states) were previously adapted to reversine in the course of 90 days (Adell & Klockner, 2023) and analyzed at three time points, after 30, 60, and 90 days. Cells were continuously cultivated in a medium containing high enough reversine concentration to provide strong selection pressure under persistent CIN. Based on this experiment, concentrations for co-culturing experiments and colony formation assays were determined. For these “short-term” experiments, lower concentrations of reversine were used for each ploidy state to obtain measurable growth. The table below shows the reversine concentration used for different cell lines and different experiments:

Cell line	Reversine concentrations	
	Co-culturing assay	Colony formation assay
Diploid HAP1	300 nM	250-300 nM
Tetraploid HAP1	/	250nM

4 Generation of stable GFP+ cell lines

To generate cell lines with stable GFP expression, the GFP must be stably integrated into the host cell genome. This was achieved via lentiviral transduction of the target cell lines.

2.1.2 Lentiviral transduction

Before transducing the target cell lines, the lentivirus carrying transgene (GFP) had to be produced. This was done by transfecting HEK293HiEx cells with an integration plasmid (expressing GFP), packaging plasmid, and envelope plasmid (See Supplementary Table 4). These three plasmids were transformed by mixing appropriate plasmid concentrations with PEI and Opti-Mem (Figure 4). Transfected HEK293HiEx cells were incubated for 3 days. After incubation, the virus-containing supernatant was collected using a 0.45-um filter. Target cells were transduced with 1:1 dilution of the virus with 4µg/mL polybrene and incubated for 3 days. If not used immediately, the collected virus was stored at −80°C for later use. Finally, transduced cells were single-sorted for GFP fluorescence. Single sorting was performed on FACSMelody (see Methods 2.2.2).

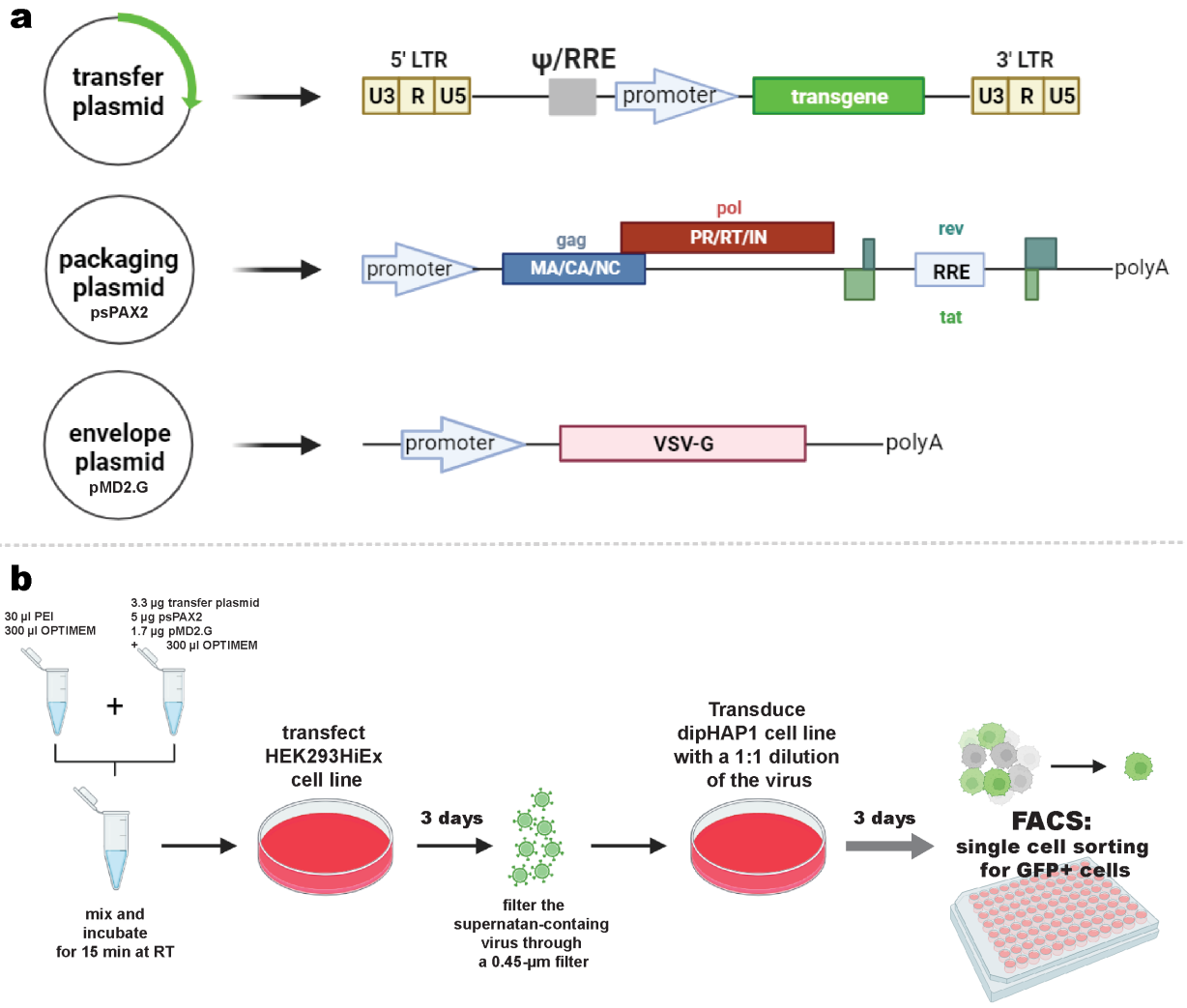

Figure 4: Lentiviral transduction for stable integration of GFP. (a) Schematic representation of the second-generation lentiviral plasmids used in these experiments. (b) Schematic representation of the experimental workflow.

After ~ 10 days, colonies were expanded from a 96-well plate into 12—and later into 6-well plates in intervals of ~3 days. After expansion, clonal populations were checked with FACSMelody for the stability of their GFP signal. Only cell lines that were stably expressing GFP were used for further experiments.

2.1.3 Fluorescence-activated cell sorting

As mentioned in the section above, to select successfully transduced (and transfected) cells, they had to be single-sorted using fluorescence-activated cell sorting (FACS). From a mixed population, we single-sorted (or bulk-sorted) for GFP-expressing cells. For all FACS experiments and all cell lines, cells were trypsinized as usual and resuspended in the medium containing PBS and 10% FBS. For single-cell sorting, cells were plated into 96-well plates, while for bulk sorting, cells were plated into 6-well plates. The growth medium for FACS-sorted cells was supplemented with normocin (1:500) (Fisher Scientific) following the first 2 d after sorting to suppress mycoplasma, bacterial, and fungal contamination. FACS was performed on a BD FACSMelody cell sorter.

2.2 Co-cultivation (competition) assay

GFP-expressing and non-fluorescent (dark) cell lines were seeded in 10 cm dishes ~2 days before FACS sorting. When cells reached ~80% confluency, the two cell lines were trypsinized and resuspended in FACS media (see 2.3) (day 0). The two cell lines were bulk sorted into 4ml of growth media supplemented with Normocin. Cells were mixed in a 50:50 ratio by bulk sorting 400,000 cells of each cell line. The gates were set up based on the parental, non-fluorescent (dark), and GFP-expressing cell lines (Figure 5). Mixed cell lines were cultured in 6-well plates, where 50,000 mixed cells were added to each well. Half of the wells were supplemented with 300 nM reversine, while the other half was a standard growth control. The remaining mixed cells were used to determine the percentages of GFP+ and dark cells at day 0 by flow cytometry. After 4 days, cell mixtures were passaged, and the relative abundance of GFP+ and dark cells was measured by flow cytometry. All later measurements were done in three to four-day intervals for a total duration of 13 - 19 days.

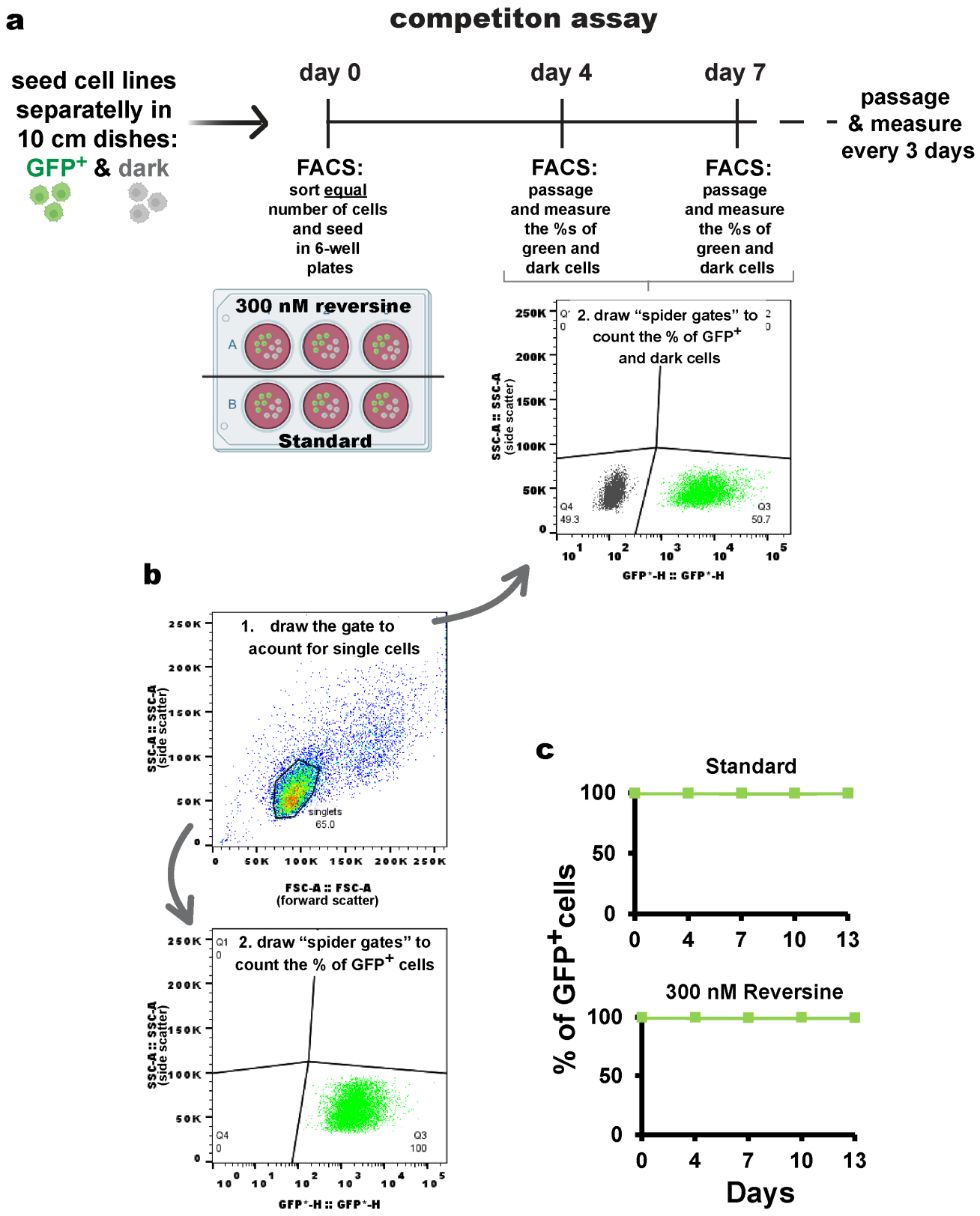

Figure 5: Competition assay for dipHAP1 cell lines. (a) Schematic overview of the competition assay. (b) Upper panel - Gate settings for accurate isolation of single cells from the population (either dark, GFP+ or mixed). Lower panel - Spider gates for counting the % of cells in a population. (c) %s of GFP+ cell line (wt dipHAP1 GFP+ (X loss)) grown over the course of 13 days under standard conditions and 300 nM reversine.

2.3 Colony formation assay

To measure the cells' general fitness and resistance to reversine, a colony formation assay was done for all adapted and engineered cell lines used in this study. On day zero, 600 cells were seeded into 6-well plates. To seed only 600 cells, the number of living cells had to be measured first. This was done by pipetting 10 ul of resuspended cells onto Countess slides, and cell count measurement was done using the Countess cell counter. Once the number of viable cells was measured, the following formulas were used to calculate the appropriate volume for seeding 600 cells:

1. (#of cells/ml) / dilution factor = # of cells/ml after dilution
- Cells had to be diluted to allow more accurate seeding.

2. (600*1000ul) / #of cells/ml after dilution = X ul of diluted sample for 600 cells in 2ml

Each cell line was grown under two conditions: IMDM++ medium supplemented with appropriate reversine concentration (+Rev) and IMDM++ supplemented with the corresponding amount of DMSO as a control (-Rev). Cells were incubated for 12 days.

Manuel used the following reversine concentrations for the adapted cell lines: dipHAP1 = 400 nM; tetHAP1 = 230-300 nM; RPE1 = 125 nM; tetRPE1 = 100-150 nM. For the engineered dipHAP1 cell lines, 300 nM reversine was used, and for the engineered tetraploid HAP1 cell lines, between 250 and 300 nM reversine was used (as written in Table 1). However, only 250 nM reversine provided measurable growth for the tetraploids (Figure 9g and h).

At day 12, colonies were fixed with 4 % (vol/vol) formaldehyde in PBS (Thermo Fisher Scientific) and incubated for 20 min, washed with purified water or PBS, stained for 20-30 min with Crystal Violet, washed with purified water several times until the dye was washed off and dried. ChemiDocMP Imaging System (Bio-Rad) was used to image the plates, and image analysis was performed using ImageJ. The same settings were used for each image and each well: known distance = 34.6 mm; threshold min = 70; max = 255; selection size: 550x550. The fraction of the area above the threshold was measured.

2.4 DNA content (ploidy) analysis by flow cytometry

To determine the ploidy state of the HAP1 cell line, cells were trypsinized and stained with 0.2 µg ml^{-1} Hoechst 33342 (Thermo Fisher Scientific) for 30 min at 37°C. Analysis by flow cytometry was done on a BD FACSAria™ IIu cell sorter (BD) using an argon laser tuned for UV (353-365 nm) and fluorescence detection at 480 nm.

2.5 Next-generation sequencing (NGS) and data analysis

All adapted and engineered cell lines were sequenced to determine their karyotype deviations, as previously described in (Adell et al. 2023 and Ravichandran et al., 2018). Subconfluent populations were pelleted, and genomic DNA was isolated using the QIAamp UCP DNA Micro Kit (Qiagen) and following the protocol provided with the kit (citation). Extracted genomic DNA was then sheared to ~500 base pairs (bp) fragments using the Bioruptor Pico sonicator (Diagenode) for two to three cycles (30 sec on/off). To check if the fragmentation was efficient, the samples were run on a 0.8 % agarose gel stained with 1µM SYTOX green (ThermoFisher). DNA libraries were prepared with the NEBNext Ultra II DNA library kit for Illumina (NEB). To isolate DNA fragments of optimal sizes AMPure XP beads (Beckman Coulter) were used. Per run, up to 96 cell lines were barcoded and multiplexed with NEBNext Multiplex Oligos (Index Primers 96-well format, NEB) and mixed at equimolar ratios. The multiplexed samples were sequenced using the Illumina HiSeqV4 SR50 setting on an Illumina HiSeq 2500 system and using the Illumina NextSeq2000 P2 SR100 setting on an Illumina NextSeq 2000 system at the Vienna Biocenter Next-Generation Sequencing Facility (VBCF). Sequencing files are available on the Sequence Read Archive (BioProject ID: PRJNA885752). The demultiplexed data sets were then aligned to the human genome (assembly: GRCh38.p12) using Bowtie2 (version 2.2.9, http://bowtie-bio.sourceforge.net/bowtie2, (Langmead and Salzberg 2012)), converted to bed files using SAMtools (version 1.3.1; http://samtools.sourceforge.net, (Li et al. 2009; Li 2011)) and Bedtools (version 2.14, http://bedtools.readthedocs.io, (Quinlan and Hall 2010)). The obtained bed files were then processed through the Gingko cloud software (Garvin et al. 2015) to correct for GC bias in low-read datasets and then analyzed with custom-made Python scripts.

2.6.1 In-depth analysis of chromosome copy number changes

For all of the adapted cell lines, we previously performed in-depth characterization of chromosome copy number changes. This is described in detail in Adell et al. 2023. Here, I will briefly introduce the workflow with blots showing examples of various copy number changes (Figure 6).

The analysis was done in 3 steps.

1. **Segmentation and change point detection**

Performed on copy number data that has been previously GC-debiased using the Gingko online tool. Binned copy number data points (single point represents 500kb) are split into segments that have equal mean copy numbers, which are categorized as: whole chromosome (no change point); a chromosome arm (one change point at the centromere, none within an arm) or a focal segment (at least one change point within a chromosome arm) (Figure 6). The PELT (Pruned Exact Linear Time) algorithm was used for change point detection (Killick et al. 2012). When the algorithm detects a change point in the

chromosome, it splits the chromosome additionally at the centromere (green dashed lines), to differentiate arm copy number changes from focal changes. Also, for all acrocentric chromosomes, only data points from q-arms were processed. Finally, the output after change point detection is a sorted list of segments.

2. **Segment assignment to corresponding wild-type segments + determination of change state (gain/equal/loss)**

To determine how and if the segment changed its state (loss, gain, or no change), it had to be assigned to a corresponding wild type. A 1-to-1 assignment was done by measuring the difference between the mean copy number values of the sample segments and the wild-type segments. Any change in the mean differences larger than 0.5 was marked as a gain, while every change smaller than -0.5 was marked as a loss. The minimum length requirement for a change to be considered was 15 data points, or 7.5 Mb.

Since the wild-type cell lines had the 'pre-existing' CNAs, these segments were excluded from further analysis of the adapted populations and, therefore, were automatically flagged. The output of this analysis step is a list of segments labeled with the change state:

- **E** = equal or no change; **G** = gain; **L** = loss
- Flagged segments were labeled with the state I (= ignore).

3. **Correction of over-segmentation**

The alignment step can lead to over-segmentation due to:

- When the change point is only present in the wild-type, it copies the change points from wild-type data to the sample data (and vice versa).
- If it finds at least one change point, it splits automatically at the centromere.

In order to correct for the over-segmentation, the sub-segments of the same change state were merged.

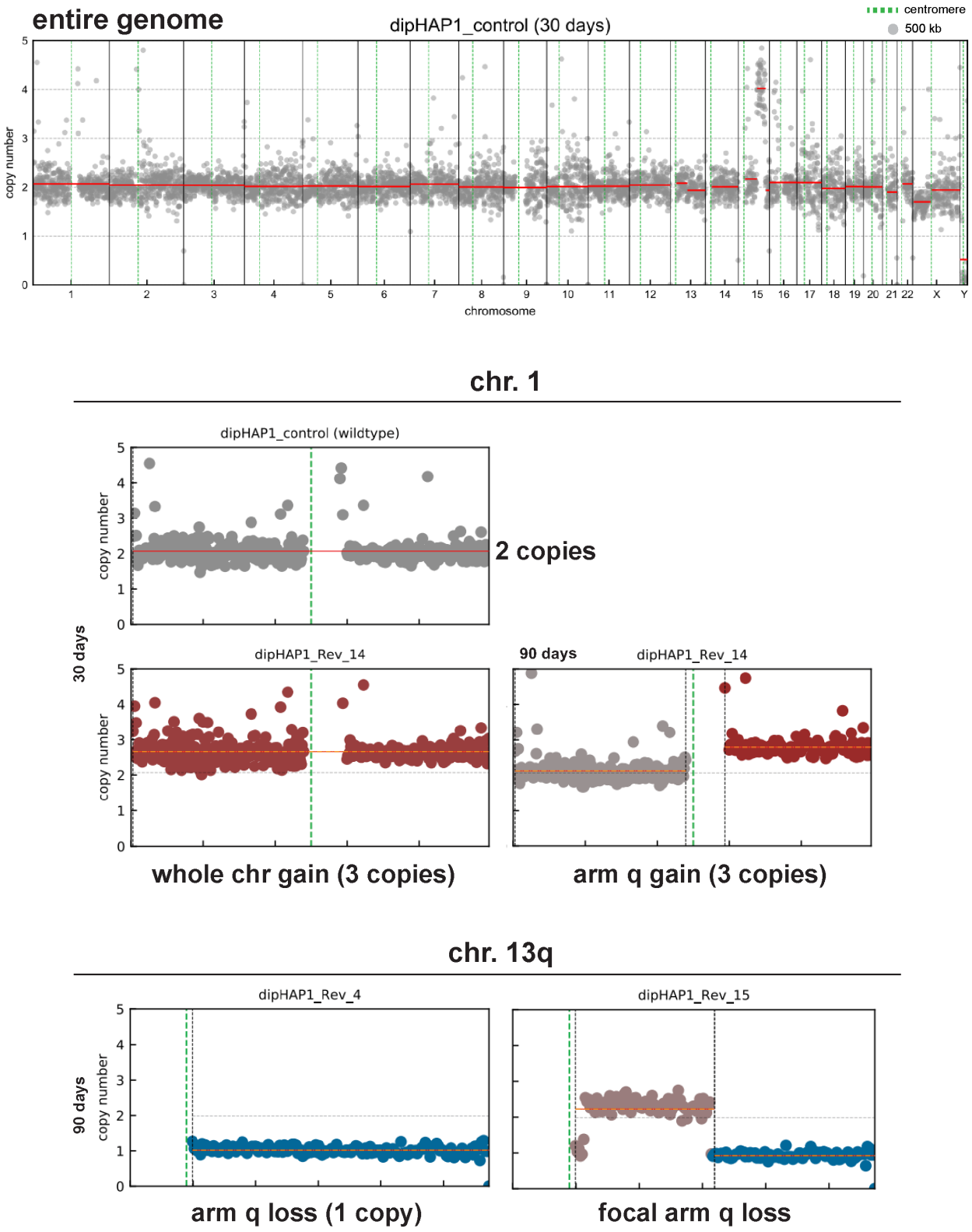

Figure 6: Analysis of chromosome copy number changes. All blots show different types of changes that occurred as a result of reversine adaptation in diploid HAP1 cell line. The first blot shows the entire karyotype of wt diploid HAP1. The lower three panels show different copy number changes of chromosome 1, while the last two blots show changes in chromosome 13q.

2.6.2 Simple analysis of adapted cell lines chromosome changes

The chromosome changes data obtained from the in-depth analysis was used to characterize the types of changes and how they differ between ploidies.

The output values are given as a number which indicates the amount of chromosome arms that given population has. In the table below all the values are described:

Ploidy state	Euploid number of chr. arms	Chr. arm gain	Chr. arm loss
Haploid	1	1.5 and higher	No losses in haploids
Diploid	2	2.5 and higher	1.5 and lower
Tetraploid	4	3.5 and higher	2.5 and lower
		4.5 and higher (not counting single arm gain)	1.5 and lower (not counting single chromosome loss)

Analysis of the percentages of chromosome arm gains and losses in different cell lines

For figures 2b, 8c, 9a and d, Supplemental Fig 1, all bar graphs show the percentage of the cell population of a certain cell line in which given chromosome arm change is present. The formula for counting in all the changes was done in excel Microsoft by using formula countif with the following from the table above.

Analysis of a single and double changes of a given chromosome arm

For figures 9d and supplemental fig 1 bar graphs that show the double gains/losses of given chromosome arms are counted using countif with the criteria for tetraploids from the table above (last row).

Gene burden analysis

The first step of this analysis was done by looking up the number of coding genes found on each chromosome arms. Next, the intrinsic aneuploidies found in the parental cell lines were excluded from the analysis. Then, for each adapted cell line, the non-binary gene

burden analysis was performed where for each change (either loss or gain of the arm or whole chromosome) the number of genes that was found on those chromosomes was counted using IF formula, with the following criteria:

=IF (value for chr. arm>4, (value for chr. Arm - 4) * number of genes on the arm, 0) → for chromosome gain

=IF (value for chr. arm<4, (value for chr. Arm - 4) * number of genes on the arm,0) → for chromosome loss

Finally, for each adapted population, the genes found on all aneuploid chromosomes were summed up and plotted as a single dot in a Fig 8a.

2.6 Engineering of full and partial chromosome arm deletions

The engineering of chromosome arm deletions in tetraploid cells utilized the CRISPR/Cas9 system as described by Ran et al. (2013), following an approach from Adell et al. (2023) and Zuo et al. (2017) (Figure 7).

2.7.1 Guide RNA design

Guide RNAs targeting repetitive sequences within the chromosome arm were selected using a custom-made Python script. Additionally, single cutting sgRNAs aimed at the intergenic region close to the centromere, were chosen based on their top-ranking results in the online tools GuideScan (Perez et al., 2017; recently updated to GuideScan2 (Schmidt et al., 2022)) and CRISPOR (Concordet and Haeussler, 2018, http://crispor.tefor.net). Off-target analysis was conducted using Cas-OFFinder from the CRISPR RGEN Tools (Bae et al., 2014, http://www.rgenome.net/cas-offinder/). Two sgRNAs that were used for engineering whole deletions of chromosome arms 13q and 6p are listed in Supplemental Table 3 and Fig.7 (from Adell et al 2023). The calculation of the number of protein-coding genes was based on the MANE project (release v1.0, Morales et al., 2022).

2.7.2 Experimental workflow

On day 0, tetraploid HAP1 wild type cell line (p53-/-/-/-) was subconfluently seeded in a 6-well plate. On the next day, transfection was carried out with 1µg of the pSpCas9(BB)-2A-GFP plasmid using XtremeGene9 (Roche):

- put DNA on ice 1h prior to transfection
- preheat Opti-Mem to 37°C, let XtremeGENE 9 (or Fugene) reach RT, vortex!

- add 3 ul XtremeGENE 9 (5 ul of Fugene) to 150 ul Opti-Mem (never touch plastic tube with tip) (incubate 5 min at RT)
- add DNA/RNA to the mix, pipette up and down (incubate 15 min at RT)
- add DNA mix dropwise to the cells
- incubate for 3 days at 37°C

72 hours post-transfection, cells expressing GFP were single-cell sorted by FACS in 96-well plates. The clonal populations were expanded in a 12-well plates and later to 6-well plates. All of the clonal populations that survived (and had growth rate similar to wild type) were frozen and stored at -80°C. In parallel, for all of the frozen clonal populations, genomic DNA was extracted using 0.5x lysis buffer (Ramlee et al., 2015). After purification, DNA was diluted to 10ng/ul for optimal qPCR normalization. DNA concentration was measured using the Qubit dsDNA HS assay (Invitrogen) following the manufacturer's protocol (1 ul sample in 198 ul buffer + 1 ul reagent measured).

To check if the clonal populations have the wanted chromosome arm deletion (either chr 6p or 13q), quantitative PCR (qPCR) was performed (Adell et al 2023; Ravichandran et al. (2018). Luna universal qPCR master mix (NEB) and 10 ng DNA from each sample were used, along with two primer pairs targeting the telomeric and centromeric regions of the respective chromosome arm (Fig. 7b, Supplemental Table 6). All qPCR reactions were performed on Mastercycler ep realplex platforms (Eppendorf). Ct values were normalized to the values of a primer pair targeting the euploid chromosome 4 (ALB control primer). Samples and controls were measured in triplicates. In addition to qPCR analysis, the karyotype of all engineered aneuploid cell lines was verified by whole-genome sequencing according to the aforementioned protocol.

The aneuploid cell lines were frozen in 4-5 aliquots. In each experimental cycle, fresh aliquots were thawed and cultured for a maximum of 6 passages, in order to avoid the formation secondary karyotypic changes.

qPCR cycle conditions:

Denaturation: 95^0C for 15sec
Annealing: 63^0C for 40sec
Elongation: 72^0C for 10min

- Prepare qPCR Mix with MasterMix (Luna) + ddH2O + DNA
- Prepare 96 well plate with 19 ul MasterMixes
- Add 1 ul Primer Mix (76 ul ddH2O + 2 ul forward primer (100uM) + 2 ul reverse primer (100 uM))

Volume per single 20 ul PCR reaction
10 ul MasterMix Luna
8 ul ddH2O

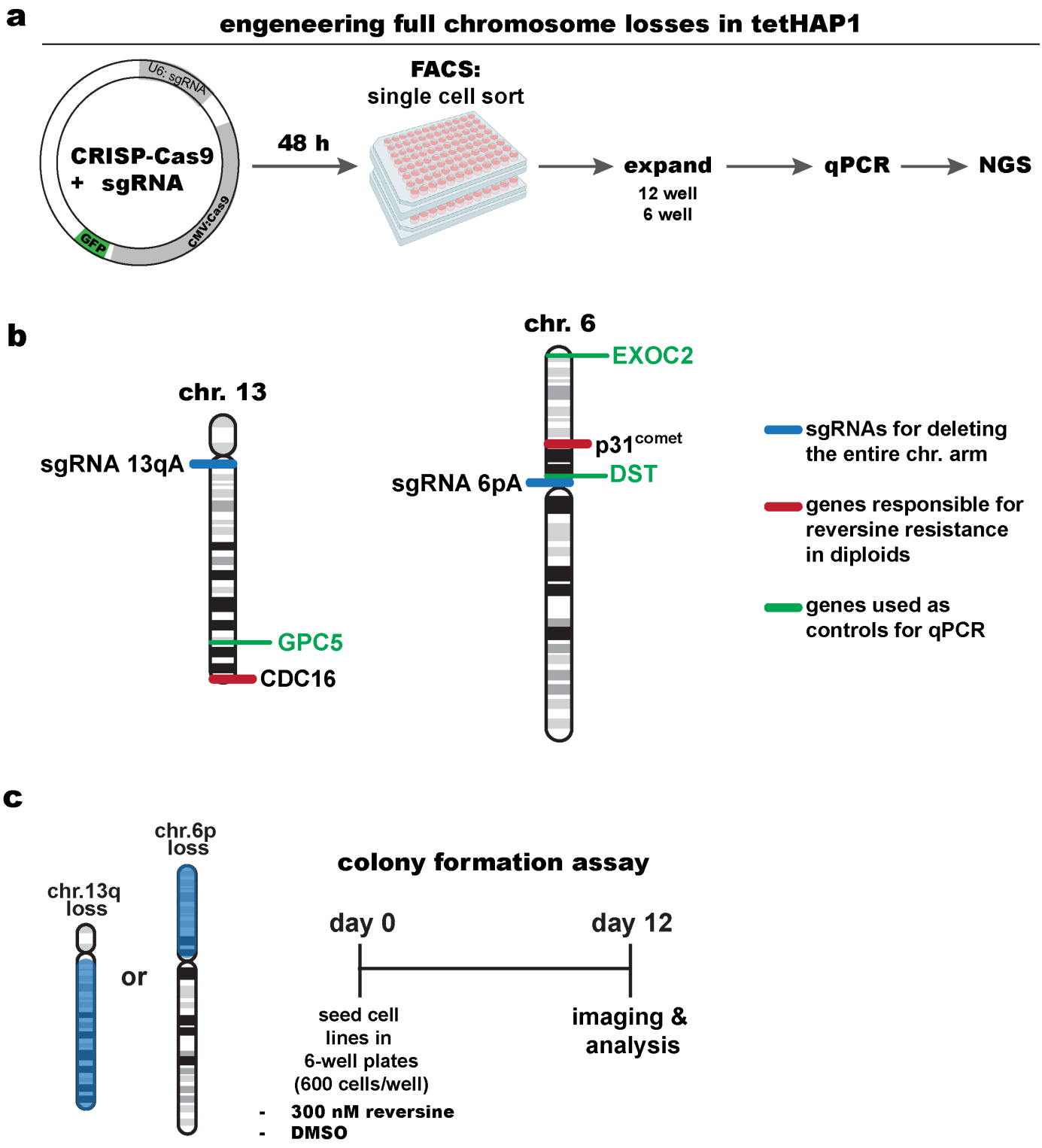

Figure 7: Engineering chromosome 6p and 13q losses in tetraploid HAP1 cell lines. (a) Schematic overview of the CRIPS-Cas9 chromosome deletion protocol (Source: Adell & Klockner). (b) Schematic representation of chromosomes 6p and 13q with depicted positions for guide RNAs (blue lines) and control genes used for qPCR (green lines). Red lines represent positions of the genes responsible for reversine resistance in diploid HAP1s (Source: Adell & Klockner). (c) Schematic overview of the colony formation assay.

2.7 Statistical analysis and sample number

All experiments were performed multiple times. Statistical analysis was carried out using Excel and GraphPad Prism software. The unpaired Student's t-test was used to assess any differences between the wild-type cell lines. Specifics regarding the statistical tests applied in a given experiment are outlined in the figure legends. Error bars depict the standard deviation (+/- SD) unless stated otherwise.

2.8 Software

- Microsoft Office Excel (2013) (Microsoft Corporation, WA, USA)
- GraphPad Prism 7 (GraphPad Software Inc.)

3. Results

3.1 Long-term MPS1 inhibition: The ploidy state dictates karyotype refinement over time by influencing the aneuploidy selection rate and specificity in HAP1 and RPE1 cell lines.

To explore how ploidy affects aneuploidy pattern formation, M.A. Adell subjected five p53-deleted cell lines to the 90-day adaptation protocol described in Adell & Klockner et al., 2023 (Adell et al., 2023) **(Figure 8a)**. As a model system, M. A. Adell selected five near-euploid human (p53 null) cell lines which fall into two categories: myeloid leukemia (HAP1; diploidized HAP1 - referred to as dipHAP1; tetraploidized HAP1 – referred to as tetHAP1) and epithelial noncancer (hTERT-RPE1 and tetraploidized hTERT-RPE1 – tetRPE1) **(see supplemental figure 1)**. The first step in the reversine-adaptation protocol was to seed multiple cultures of parental cell lines and preincubate them in a medium containing reversine for 3 days. After preincubation, single-cell sorting was performed to obtain clonal populations, which were then cultivated in reversine for 90 days. For each of the five parental cell lines, at least 20 clonal populations were cultivated in reversine. In parallel with the adaptation protocol, six clonal populations per parental cell line were grown without reversine (standard conditions) in order to follow the karyotype stability of these cell lines over time. To analyze the karyotypic changes and fitness of the adapted cell lines, low-coverage whole-genome sequencing (Illumina NGS, **Methods 2.5, Figure 6, Source: M. A. Adell published and unpublished data**) was performed, together with colony formation assays at 30-day intervals. This adaptation protocol allowed for the identification of recurring aneuploidies in both HAP1 and RPE1 cell lines and their different ploidy states (haploid, diploid, and tetraploid).

As reviewed by Ben-David and Amon (Ben-David & Amon, 2020), aneuploidy is defined as a change in the copy number of the whole chromosome or whole chromosome arm. However, our analysis of somatic copy number alterations in the reversine-adapted cell lines included changes in whole chromosomes, whole chromosome arms, and focal changes. Copy number was measured relative to the untreated parental population in 7.5-Mb intervals **(Figure 6, Methods 2.6.1)**. This data from the whole genome

sequencing of all adapted cell lines gave us multiple insights about the process of complex karyotype formation across ploidies.

Firstly, the complexity of karyotypic changes is greater in a higher ploidy state. Diploid HAP1 cells display greater karyotypic complexity than haploid HAP1 cells, showing more chromosome arm gains and positive selection for losses of specific arms (e.g., 13q and 14q). In haploids, chromosome losses cannot be positively selected since having no copy of any of the 23 chromosomes is detrimental to the cell. Similar results were observed when comparing diploid and tetraploid cells of both HAP1 and RPE1 lineages (dipHAP1 vs. tetHAP1 and dipRPE1 vs. tetRPE1): higher ploidy states consistently exhibited a greater number of chromosome gains and losses **(Figure 8b and c).**

Secondly, we could see differences in the rate of aneuploidy formations across ploidy states. For example, in haploid HAP1s, after 90 days of reversine adaptation, on average, only ~8% of the genome is aneuploid. For diploid HAP1s and RPE1s, at 90d, this number goes up to 16% and 23%, respectively. Finally, in tetraploids already at 30 days, the average percentage of aneuploidies reaches 48% in tetHAP1s and 43% in tetRPE1s. This clearly shows how the rate of complex karyotype formation increases with ploidy increase.

Interestingly, in tetraploids, the percentage of average aneuploidies reaches its maximum already at 30 days for tetHAP1 and at 60 days for tetRPE1. In contrast, in haploid and diploid backgrounds, the percentage of average aneuploidies increases over time, reaching its maximum at 90 days. These observations demonstrate that higher ploidy levels correlate with more rapid and pronounced aneuploidy formation over time. Notably, tetraploids exhibit an earlier plateau in aneuploidy accumulation than haploid and diploid cells.

The third observation concerns the specificity of aneuploidy occurrence. Namely, independent of the ploidy state, some chromosomes are either only lost or only gained. For example, across all three ploidy states in HAP1s, chromosome arms 1q, 20q, and whole chr. 8 are always gained and never lost. In diploid and tetraploid HAP1s, chr. arms

13q and 14q are only lost. Furthermore, in diploid and tetraploid RPE1s, chr. arms 5p, 5q, 8q; whole chr. 9 and 20 are only gained, while chr. arm 6p is always lost. Finally, when we look for the common aneuploidies across two cell lines and their different ploidy states, chr. arms 8q and 20q are always gained **(Figure 8b and Supplemental Fig. 2a).**

Lastly, the sequencing data allowed us to analyze the prevalence of different types of copy number changes (whole chromosome, chromosome arm, or focal) in the adapted populations and how these change over time **(Figure 8d)**. A comparison of aneuploidy prevalences in diploid and tetraploid HAP1s showed a transition from whole chromosome changes to more arm changes over time. Namely, in both ploidy states, at 30 days of adaptation,>50% of all copy number alterations are accounted as whole-chromosome change. Already at 60 days, the number of whole-chromosome changes decreases down to <30%. Over time, the proportion of whole-chromosome aneuploidy decreased while arm and focal CNAs increased. For instance, in diploid HAP1s, trisomy of whole chromosome 1 was present in ~20% of adapted populations at day 30. After 60 days, almost 50% of the adapted populations gained only 1q arm, and it remains so by day 90 **(Figure 8b, Supplemental 2a and b**). A similar scenario has been observed in the adaptation of tetraploid HAP1s with the difference in the selection rate. Namely, already at 30 days, more than 80% of the adapted tetraploid populations had a gain of whole chromosome 1. At 60 days, 1q gain was present in more than 20% of populations, reaching ~45% by day 90. Regarding RPE1s, chromosome 6 monosomy transitioned to monosomy of just the 6p-arm in both diploids and tetraploids, while the selection of only 6p arm loss was slower in tetraploids **(Figure 8b).**

The rate of focal changes in adapted diploid and tetraploid HAP1s and diploid RPE1s gradually increases over time **(Figure 8d).** However, in tetraploid RPE1s, the most focal changes were observed at 60 days, with a decrease by day 90.

Overall, tetraploidy leads to more complex karyotype formation due to adaptation to long-term MPS1 inhibition. This complexity is reached faster than in diploids or haploids, while some specificity remains conserved over time.

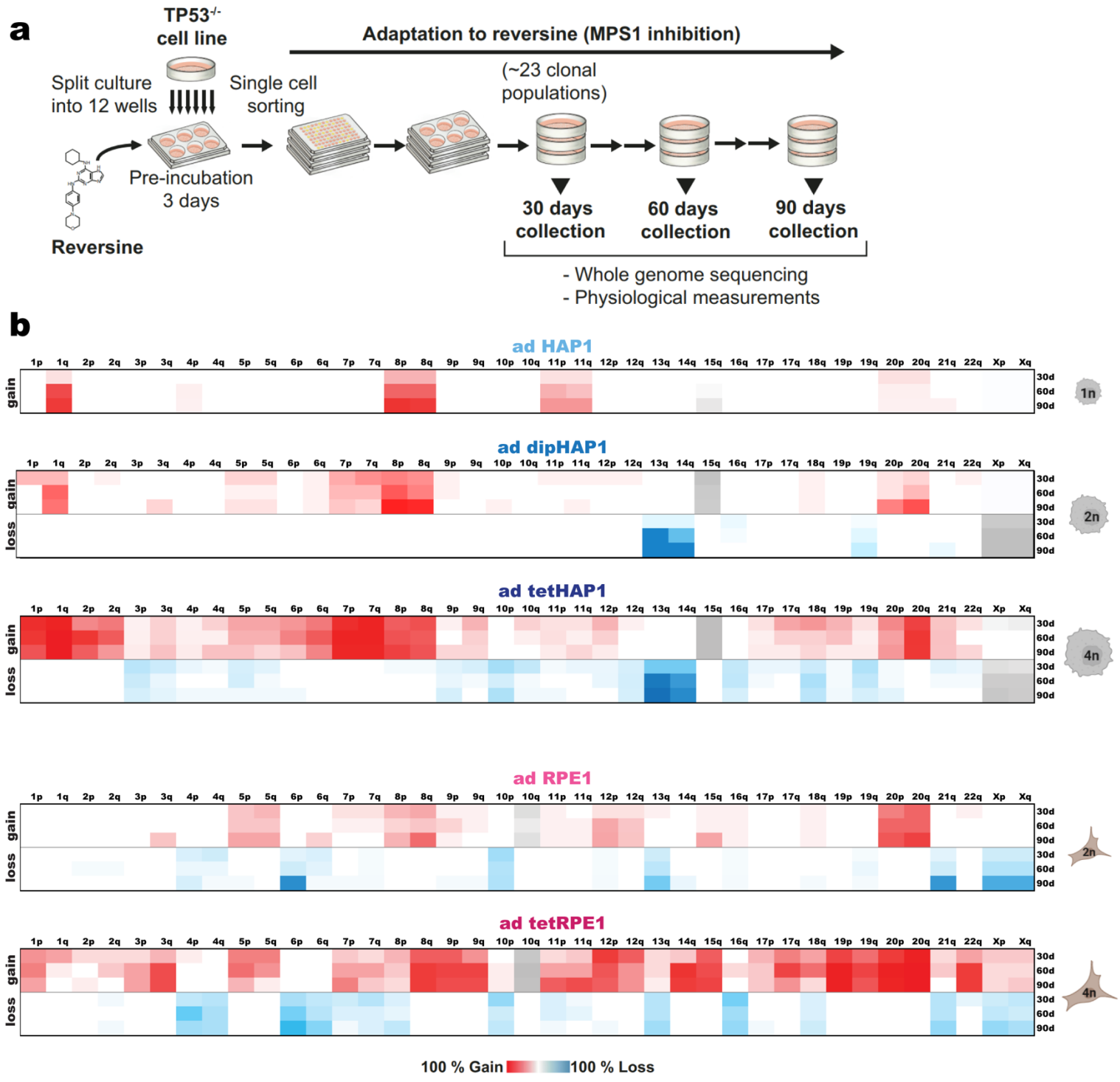
a
TP53-/- cell line
Adaptation to reversine (MPS1 inhibition)
Split culture into 12 wells
Single cell sorting
(~23 clonal populations)
Pre-incubation 3 days
Reversine
30 days collection
60 days collection
90 days collection
- Whole genome sequencing
- Physiological measurements
b
ad HAP1
ad dipHAP1
ad tetHAP1
ad RPE1
ad tetRPE1
gain
loss
30d
60d
90d
1n
2n
4n
100 % Gain
100 % Loss
c
average of all aneuploid chr. arms (%)
60.00%
50.00%
40.00%
30.00%
20.00%
10.00%
0.00%
HAP1
dipHAP1
tetHAP1
RPE1
tetRPE1
30d 60d 90d
d
ad dipHAP1
ad tetHAP1
ad RPE1
ad tetRPE1
abundance (%)
100%
75%
50%
25%
0%
30
60
90
whole arm focal

Figure 8: Long-term MPS1 inhibition: Ploidy state dictates karyotype refinement over time by influencing aneuploidy selection rate and specificity in HAP1 and RPE1 cell lines. (a) Schematic representation of the reversine adaptation process **(Source: Adell & Klockner)** . (b) Heat maps of 5 cell lines showing the mean percentage of copy number changes in chromosome arms from all populations of each adapted cell line at 30, 60, and 90 d. Chromosome gain is shown in red, and chromosome loss is shown in blue. In gray are shown the cell line-inherent aneuploidies that were present at time point 0 before the adaptation **(Source: Adell, published and unpublished data)**. (c) Average aneuploidies per adapted cell line given in percentages. Averages of all aneuploid chromosomes present in adapted populations were taken by summing up all aneuploid chromosome arms present in each population and divided by all chromosome arms that were considered. (d) Percentages of copy number changes of whole chromosomes (dark grey), chromosome arms (light grey), and segments (focal changes; empty) for all adapted cell lines at 30, 60, and 90 days.

3.1.2 Analysis of most prominent aneuploidies in all five cell lines

Next, I analyzed the most prominent aneuploidies across all ploidy states of reversine-adapted HAP1 and RPE1 cell lines. This was done by analyzing whole chromosome and chromosome arm copy number alterations. **Figure 8 and Supplemental Figure 2** show that some of the most prominent aneuploidies are present in both HAP1s and RPE1 and across all ploidy states. Such examples include gains of chromosome arms 8q, 20q, and loss of 13q arm. This suggests that the selection of these chromosomes is reversine-specific. Gains of 1q and losses of 14q in HAP1s show cell type-specific patterns. Of course, 14q loss is limited to diploid and tetraploid backgrounds since all chromosome losses are detrimental in haploids. Furthermore, 6p, 21q, and X losses are quite prominent in RPE1, both diploid and tetraploid.

As pointed out in Figure 1, the rate of aneuploidy acquisition in the adaptation of tetraploids is much greater than in haploids or diploids. For this reason, I further investigated the degree of aneuploidy of most occurrent chromosomes or chromosome arms. This was done by analyzing the percentage of single, double, or more copy number changes of a single chromosome or chromosome arm (see **Supplemental Fig 2**). For chromosome 8 gains in tetHAP1s and 18p in tetRPE1s, adapted cells tend to gain two

copies of these arms over time, respectively (Supplemental Fig 2b). The same is true for the gain of chromosome 20 in tetRPE1 but at a slower rate.

In conclusion, the analysis of aneuploidies in reversine-adapted HAP1 and RPE1 cell lines shows distinct patterns of chromosome gains and losses that are specific to each cell type or associated with reversine adaptation. Additionally, the complexity of these patterns is greater in tetraploid cells.

3.2 Adaptation mechanisms to long-term MPS1 inhibition vary depending on the ploidy and cell type.

As chromosomes consist of specific genes, aneuploidies of different chromosomes or chromosome arms (losses and gains) can be represented as the gene burden of each adapted population. In other words, gene burden analysis gives us the number of all genes that deviate from euploid in each adapted population.

From the whole genome sequencing (WGS) data, we were able to perform a 'non-binary gene burden analysis' for each adapted population of each five cell lines (see **Methods 2.5, Fig. 7a**). In short, the non-binary gene burden analysis was done by multiplying the copy number of each chromosome arm (values obtained from WGS) with the number of genes present on that arm (values obtained from NCBI). All analyzed genes were normalized to the non-adapted wild-type karyotype.

As seen in **Figure 9a,** four out of five adapted cell lines (HAP1, dipHAP1, tetHAP1, and RPE1) show a gradual increase in the number of the aneuploid genes (gained and lost) over time. The only exception is seen in adapted tetraploid RPE1 populations, where the highest gene burden is reached at day 60, and it gets reduced at 90 days. This is in line with **Figure 8c**, where the amount of aneuploid chromosomes is reduced at 90 days of adaptation in tetRPE1.

As expected, the overall number of affected genes increases with a higher ploidy state, which is in line with previous observations **(Figure 8b and c)**. Additionally, in the case of

adapted haploid, diploid, and tetraploid HAP1s, the median change from 30 to 90 days is greater in adapted populations of lower ploidy state, which is also in line with previous observations regarding differences in the rate of complex karyotype formations across ploidies **(Figure 8b)**.

Furthermore, to analyze the fitness of the adapted cell lines in reversine, M. A. Adell performed colony-formation assays (CFAs) (**Methods 2.2**). Adapted cell lines were seeded in low numbers under reversine and standard conditions. After 12 days, formed colonies were counted, and the numbers of colonies formed under reversine (+Rev) were normalized to the number of colonies formed in standard conditions (-Rev). This gave us the relative (+Rev/−Rev) growth percentages of adapted cell lines. As shown in **Figure 9b**, four out of five adapted cell lines (HAP1, dipHAP1, tetHAP1, and RPE1) showed a gradual increase in reversine resistance over time. The proliferation of cells in reversine increased from 5%–10% relative to untreated cells before the adaptation (time point 0) to ~13%–25% at 90 d. In line with gene burden analysis, in colony formation assays, tetraploid RPE1s do not show a gradual resistance increase, so, at day 90, they grow slightly worse than at day 60 **(Figure 9).**

When observing the non-binary gene burden analysis of adapted tetraploid HAP1 populations, we can see that the number of affected genes has not drastically changed over time (compared to diploids or haploids). However, looking at the growth data, the transition from time point 60 to 90 days shows a quite high increase in fitness, going from only ~8% of surviving cells at 60 days to ~25% at 90 days. This evidence indicates the underlying mechanism responsible for the increased reversine resistance in these tetraploid cell lines. As tetraploid background tolerates single and double chromosome arm losses, in the next step, I analyzed all aneuploidies that lead to more than one copy number change for both gains and losses.

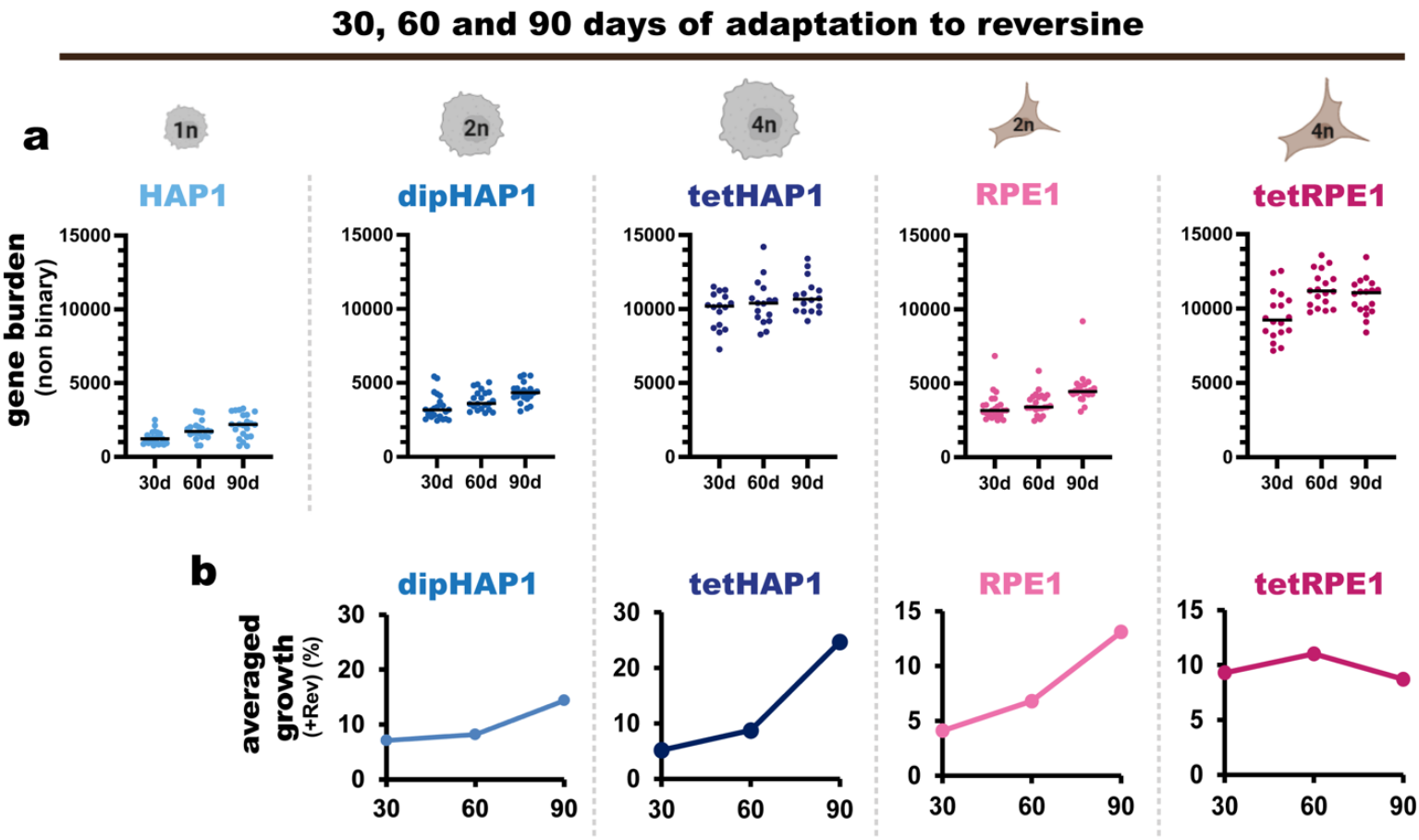

Figure 9: Adaptation mechanisms to long-term MPS1 inhibition vary depending on the ploidy and cell-type. (a) Non-binary gene burden of 5 cell lines and all their adapted populations at 30, 60, and 90d. For each adapted population, all chromosome gains and losses were accounted and the number of coding genes on these chromosomes was summed up and plotted as a single dot. (b) Growth averages of all populations of each cell line at 30, 60, and 90d as measured using colony formation assays under reversine. The percentages are normalized to the growth of the parental cell lines in the absence of reversine.

3.3 13q loss in diploid and tetraploid HAP1s.

One of the most prominent aneuploidies in adapted diploid HAP1s was the loss of the 13q arm. While 14q arm loss was defined as a cell-type specific aneuploidy, loss of 13q arm showed a correlation with better growth under reversine (Adell et al., 2023) **(Figure 10a).** In the upper graph in **Figure 10a**, Adell & Klockner saw that already at 60 days of reversine adaptation, ~90% of populations lost one copy of the 13q chr arm. To confirm the effect this aneuploidy has on the reversine adaptation of diploid HAP1s, T. Klockner engineered chromosome 13q loss in wild-type diploid HAP1 (not adapted to reversine).

This was done by performing CRISPR-Cas9 chromosome deletions. Guide RNAs were designed to cut at the repetitive sequences of the chromosome region near the centromere to induce full arm deletions (See Adel et al 2023, **Methods, Figure 7**). Now, we wanted to see whether the 13q loss in non-adapted dipHAP1 is sufficient for reversine resistance that was prominent in the adaptation process. To directly compare the fitness of the 13q loss dipHAP1 engineered cell line under reversine, I performed a co-culturing assay (**Methods 2.2.,** done based on paper (Lukow et al., 2021)). In this assay, the engineered 13q loss cell line was grown in the same dish with wild-type GFP-positive dipHAP1 (euploid for 13q). An equal number of both cell lines were seeded in the same well and grown under two conditions: standard (no reversine) and 300 nM reversine. As shown in **Figure 10b** (two upper graphs, also see **supplemental figure 3**), the cell line with engineered 13q loss quickly overtakes under reversine, while the wild type grows better under standard conditions, suggesting that 13q loss indeed provides resistance to reversine. Further investigation of 13q loss led to identifying a gene, CDC16, a member of the anaphase-promoting complex/cyclosome (APC/C). With colony formation assays, T Klockner showed that heterozygous mutation of CDC16 in dipHAP1 provides resistance when exposed to reversine. Further proof of the rescue was shown in the competition assays, performed with culturing CDC16 heterozygous dipHAP1 with GFP+ wild type **(Figure 10b and supplemental figure 3)**. In conclusion, losing a member of APC/C allows cells to delay anaphase onset and extend mitosis to limit CIN.

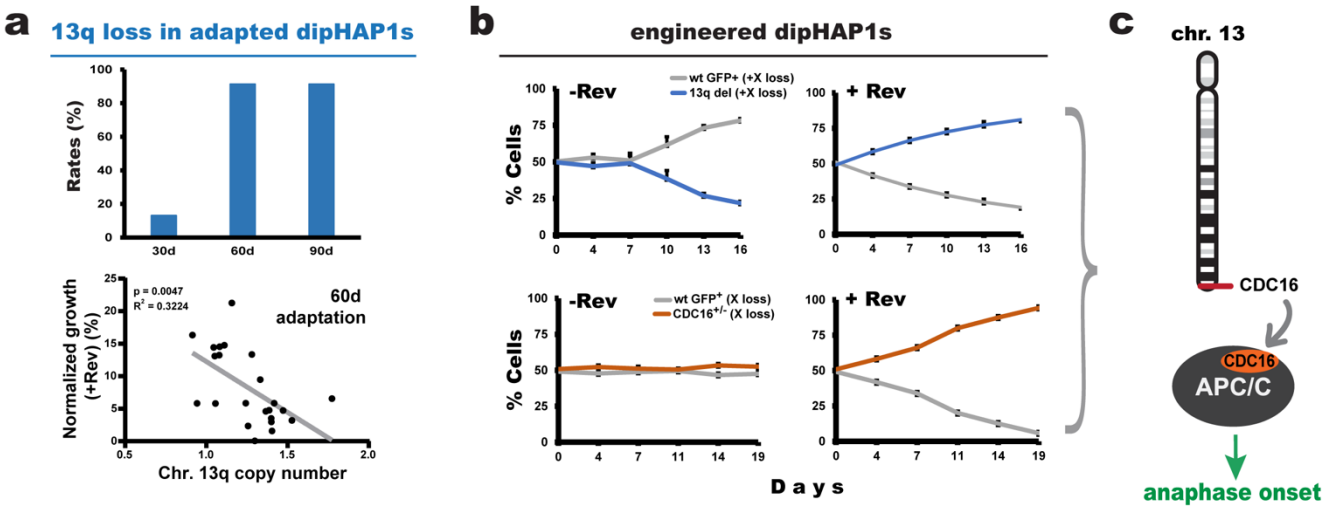
a
13q loss in adapted dipHAP1s
Rates (%)
30d
60d
90d
p = 0.0047
R² = 0.3224
60d
adaptation
Normalized growth (+Rev) (%)
Chr. 13q copy number
b
engineered dipHAP1s
-Rev
+ Rev
wt GFP+ (+X loss)
13q del (+X loss)
% Cells
wt GFP+ (X loss)
CDC16+/- (X loss)
Days
c
chr. 13
CDC16
APC/C
anaphase onset

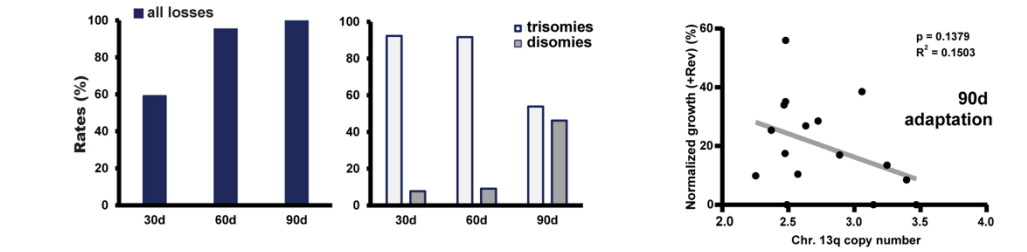
d
13q losses in ad tetHAP1
all losses
Rates (%)
30d
60d
90d
trisomies
disomies
p = 0.1379
R² = 0.1503
90d
adaptation
Normalized growth (+Rev) (%)
Chr. 13q copy number

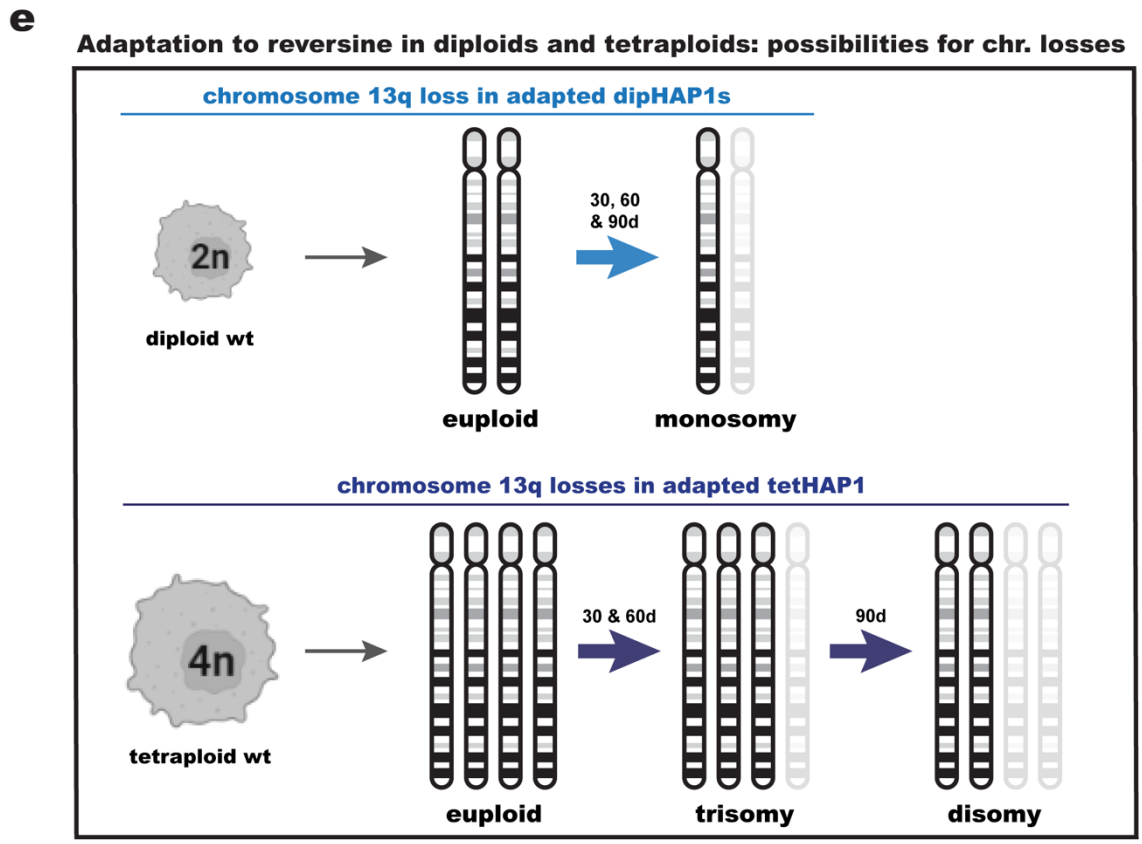
e
Adaptation to reversine in diploids and tetraploids: possibilities for chr. losses
chromosome 13q loss in adapted dipHAP1s
2n
diploid wt
30, 60
& 90d
euploid
monosomy
chromosome 13q losses in adapted tetHAP1
4n
tetraploid wt
30 & 60d
90d
euploid
trisomy
disomy

Figure 10: 13q loss in diploid and tetraploid HAP1s. (a) 13q loss in adapted diploid HAP1s. The upper bar graph shows the percentage of adapted populations containing 13q arm losses at 30, 60 and 90 days of reversine adaptation. The lower graph shows a scatter plot of adapted populations harboring 13q loss (2 indicates no loss and 1 indicates chromosome loss; X-axis) versus their normalized (+Rev) growth (Y-axis). Growth from colony formation assays was normalized to the untreated parental cell lines (WT). n = 2. Data for chromosome loss copy number are from read frequencies using Illumina sequencing. P-values are from F-tests. (b) Co-cultivation of a dipHAP1 cell line with monosomies of both X and 13q and GFP-labeled cell line with the monosomy of chromosome X with and without reversine. The mean ± SD for six separate populations of cells in one time course is shown. (c) Simplified model of the CDC16 role in reversine adaptation (Source: Adell & Klockner). (d) From left to right: First bar graph shows the percentages of adapted populations of tetraploid HAP1 cell line with all 13q losses at 30, 60 and 90 days of reversine adaptation. The second bar graph shows the percentages of adapted tetraploid populations with chromosome 13q trisomies vs disomies at 30, 60 and 90 days of reversine adaptation. Third graph shows scatter plot of adapted tetraploid populations harboring 13q loss (4 indicates no loss, and values from 3.5 to 2 indicate various degree of chromosome losses; X-axis) versus their normalized (+Rev) growth (Y-axis). Growth from colony formation assays was normalized to the untreated parental cell lines (WT). n = 2. Data for chromosome loss copy number are from read frequencies using Illumina sequencing. P-values are from F-tests. (e) Possibilities for chromosome losses in tetraploid background on an example of chromosome 13q.

In **Figure 9b,** we saw that the fitness of adapted tetraploid HAP1 drastically increases from day 60 to day 90 of adaptation, while the number of affected genes does not follow this trend. This potentially points to the development of some other resistance mechanism that might be unique to tetraploidy. To understand this, I analyzed single (trisomies) or double (disomies) chromosome arms losses in ad tetHAP1 since tetraploid background allows for more varieties in aneuploidy status of same chromosome arms **(see Figure 10e, supplemental figure 2)**. Indeed, as pointed out in the result section **3.1**, the rate of acquired chromosome losses at day 30 is higher in tetraploids than in diploids, which is also shown in the analysis of chromosome 13q losses. However, in both ploidy states, this chromosome arm loss is present in nearly 100% of adapted cell lines already by day 60. The main difference is that by day 90 of reversine adaptation, tetraploid HAP1s transition from single 13q arm loss to double losses, where already ~50% of ad tetHAP1 have lost more than one 13q arm **(Figure 10d)**. When analyzing the correlation of different 13q losses with growth (+Rev) of ad tetHAP1, we saw no significant impact. The lack of significant impact of 13q arm loss on cell growth under reversine may be attributed to the

accumulation of many other aneuploidies in the adapted tetraploid cells, which likely buffer out any potential effects of 13q loss. For this reason, we decided to introduce various degrees of chr. 13q arm deletion in non-adapted tetHAP1 to test the differences in fitness impact.

3.4 Engineered individual chromosome deletions in a tetraploid background result in the formation of additional changes but can still recapitulate reversine resistance.

As mentioned in the previous section, Adell & Klockner showed the impact of engineered 13q and 6p losses on reversine resistance in diploid HAP1 cell lines (Adell et al., 2023). Here, I wanted to see this impact in the tetraploid background by implementing the same CRISP-Cas9-induced chromosome arm losses. As pointed out, tetraploidy allows multiple possibilities for chromosome losses by tolerating one or two chromosome arm deletions. Here, a wild-type tetraploid HAP1 cell line was used for arm deletions **(supplemental figure 4, methods 2.6)**. To do this, this cell line was transfected with a plasmid that contains Cas9 and guide RNA sequences (either 13q guide or 6p guide), and after 72 hours (time needed for sufficient cut), cells were single-sorted. After expansion, qPCR analysis allowed us to determine which clones have a deletion of 13q or 6p arms **(Figure 11a and f, supplemental figure 4)**. Each clonal population that showed reduced signal in qPCR analysis was sent for whole-genome sequencing to check the entire karyotype **(Figure 11b and f, supplemental figure 4)**. In each engineered clonal population, this procedure resulted in many other aneuploidies that are not the focus of this project. However, for each chromosome arm deletion, I chose two engineered cell lines which had the least number of 'unwanted' aneuploidies, and performed colony formation assays under reversine, to validate the impact of 13q and 6p losses. Based on qPCR and NGS data, in both cases (13q deletion and 6p deletions), one of the two chosen cell lines had single arm deletion (tet13q #36 and tet6p #26), while the other had deletions of two copies of the respected arm (tet13q #45 and tet6p #30) **(Figure 11).** For colony formation assays, we compared the growth of engineered tetraploid cell lines with tetraploid wt, diploid wt, and diploid engineered. In each well, 600 cells of specific cell line were seeded, once in

standard condition and once in reversine (250 nM for tetraploids; 400 nM for diploids). After 12 days, colonies were stained and analyzed. As shown in **Figure 11d and h**, engineered tetraploid cell lines show a similar degree of resistance as diploids. When comparing the impact of single arm deletion vs double, we can see that double deletions (disomies) of both 13q and 6p arms show higher resistance than single deletions in a tetraploid background. This aligns with observations that the additional loss of the 13q arm facilitates further reversine adaptation in the adapted tetraploid HAP1s (see section **3.3**).

.

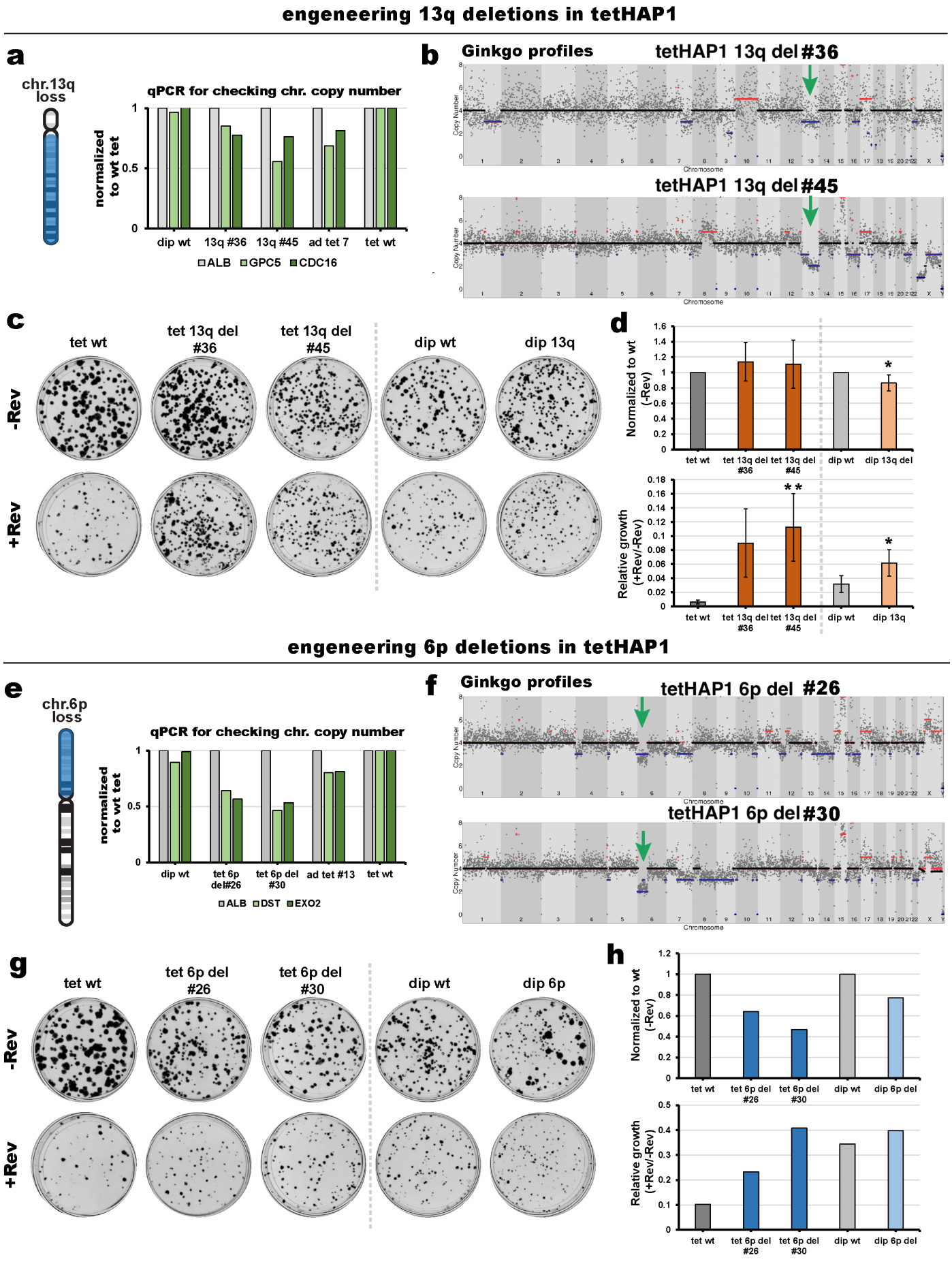
engeneering 13q deletions in tetHAP1
a
chr.13q loss
qPCR for checking chr. copy number
normalized to wt tet
dip wt
13q #36
13q #45
ad tet 7
tet wt
ALB
GPC5
CDC16
b
Ginkgo profiles
tetHAP1 13q del #36
tetHAP1 13q del #45
Copy Number
Chromosome
c
tet wt
tet 13q del #36
tet 13q del #45
dip wt
dip 13q
-Rev
+Rev
d
Normalized to wt (-Rev)
Relative growth (+Rev/-Rev)
tet wt
tet 13q del #36
tet 13q del #45
dip wt
dip 13q del
engeneering 6p deletions in tetHAP1
e
chr.6p loss
qPCR for checking chr. copy number
normalized to wt tet
dip wt
tet 6p del#26
tet 6p del #30
ad tet #13
tet wt
ALB
DST
EXO2
f
Ginkgo profiles
tetHAP1 6p del #26
tetHAP1 6p del #30
Copy Number
Chromosome
g
tet wt
tet 6p del #26
tet 6p del #30
dip wt
dip 6p
-Rev
+Rev
h
Normalized to wt (-Rev)
Relative growth (+Rev/-Rev)
tet wt
tet 6p del #26
tet 6p del #30
dip wt
dip 6p del

Figure 11: Engineered individual chromosome deletions in tetraploid background results to formation of additional changes but can still recapitulate reversine resistance. (a) qPCR results of the engineered 13q loss in tetraploid cell line. Values are firstly normalized to reference gene albumin (ALB – on chr 4) and then to tetraploid wt GPC5 and CDC16 values (both on chromosome 13q (see Methods). (b) Copy number profiles of engineered tetHAP1 cell lines with the deletion of chromosome arm 13q. Blue dots represent the region of chromosome loss, which is highlighted with a green arrow. (c and g) Colony formation assay results, upper row shows cells grown under normal conditions, lower row shows cells grown under reversine. (d and h) Proliferation measurements are from colony formation assay. Normalized (−Rev) and relative (+Rev/−Rev) growth of the depicted 13q or 6p cell lines and wt controls. Upper bar graph: normalized growth (−Rev) represents the growth of the cell line without reversine normalized to the growth of the wt tetraploid or diploid HAP1 without reversine. The relative growth (+Rev/ −Rev) represents the growth of the cell line with reversine (+Rev) relative to its growth without reversine (−Rev). The dotted line separates tetraploid and diploid cell lines since each were normalized to their own parental cell line. In d bars depict mean ± SD (n = 5). P-values are from unpaired Student's t-tests. (∗) $P < 0.05$, (∗∗) $P < 0.01$, (∗∗∗) $P < 0.001$, (∗∗∗∗) $P < 0.0001$. Where not indicated, the P-value was > 0.05. (e) qPCR results of the engineered 6p loss in tetraploid cell line. Values are firstly normalized to reference gene albumin (ALB – on chr 4) and then to tetraploid wt GPC5 and CDC16 values. (f) Copy number profiles of engineered tetHAP1 cell lines with the deletion of chromosome arm 6p. Blue dots represent the region of chromosome loss, which is highlighted with a green arrow.

4. Discussion

In my master's thesis project, I analyzed complex karyotype formation in haploid, diploid, and tetraploid HAP1 cell lines, as well as in diploid and tetraploid RPE1 cell lines that had been previously adapted to the long-term chromosome instability-inducing drug reversine. By analyzing growth and next-generation sequencing data, I was able to highlight some differences and similarities in the adaptation process across different ploidy states. Furthermore, I determined the impact of chromosome 13q and the gene CDC16 on reversine resistance in the diploid HAP1 cell line. Finally, using CRISPR/Cas9, I engineered chromosome losses of 13q and 6p in the tetraploid HAP1 cell line to assess the degree of reversine resistance within this tetraploid background.

4.1 The ploidy state dictates karyotype refinement over time by influencing aneuploidy selection rate and specificity in HAP1 and RPE1 cell lines.

The formation of complex karyotypes in cancer is influenced by various factors, including cell type, chromosome size, essential genes, and the ploidy state of the cell (Baker, Waise, et al., 2024; Beroukhim et al., 2010; Bigner et al., 1990; Bochtler et al., 2019; Selmecki et al., 2015; Zack et al., 2013). In this study, we concentrated on the influence of ploidy on aneuploidy selection amid continuous chromosomal instability (CIN). This was investigated by subjecting *two* human cell lines with different ploidy states to a 90-day CIN adaptation protocol outlined in Adell & Klockner et al., 2023. High rates of CIN were achieved through reversine treatment, which inactivates the spindle assembly checkpoint, creating selective pressure under which cells undergo various karyotype alterations. This protocol enabled us to examine how the ploidy state affects karyotype refinement in adapted human cell lines, comparable to previous findings from the adaptation of haploid and diploid yeast strains previously conducted in our lab (Ravichandran et al., 2018).

To explore the role of ploidy in complex karyotype formation in human cell lines, A. Adell *used* the HAP1 cell line in three ploidy states: haploid, diploid, and tetraploid, along with the RPE1 cell line in two ploidy states: diploid and tetraploid. Throughout their evolution, these cells developed distinct karyotype patterns influenced by their initial ploidy states and exposure to reversine **(Figure 8b)**. As previously demonstrated in yeast, the impact of individual chromosome copy number alterations is buffered in higher ploidy states; concurrently, the level of aneuploidy increases with an increase in the cell's ploidy (Beach et al., 2017; Ravichandran et al., 2018; Selmecki et al., 2015). Consistent with this and analysis of aneuploidy in different human tumor types (Prasad et al., 2022), we report that the average degree of wide range-aneuploidy rises with an increase in ploidy in both HAP1 and RPE1 cells **(Figure 8c)**. Specifically, a haploid background permits only chromosome gains; diploids tolerate only certain chromosome losses. In contrast, tetraploids can significantly expand their chromosome copy number changes (both gains and losses) **(Figure 8b).** This aligns with observations by Baker 2024, which indicated that higher ploidy states have a more significant impact on patterns of chromosome losses than gains (Baker, Lai, et al., 2024). Additionally, Adell and Klockner highlight aneuploidy refinement in adapted diploid cell lines, where they noted a shift from whole chromosome changes to chromosome arm changes over time (Adell et al., 2023). A similar pattern is observed in tetraploids **(Figure 8d)**. Furthermore, tetraploidy significantly impacts the rate of aneuploidy selection, revealing a clear contrast with lower ploidies. This observation also highlights the improved ability of tetraploid cells to tolerate changes in chromosome copy number (Dewhurst et al., 2014).

4.2 Adaptation mechanisms to long-term MPS1 inhibition vary depending on the ploidy and cell type.

Even though the number of aneuploid genes increases with ploidy increase **(Figure 9)** (Kuznetsova et al., 2015; Prasad et al., 2022; Ravichandran et al., 2018), here I could point out that different cell-types have different mechanisms of adaptation to CIN. Namely, the complex karyotype refinement strategies vary in multiple ways. Firstly, tetraploidy did not affect the specificity of the selection of specific aneuploidies. For example, the loss of

chromosome 6p is typical for RPE1 independent of its starting ploidy state; the same is true for the loss of chromosome 14q in diploid and tetraploid HAP1s **(Figure 8).** Secondly, an interesting adaptation mechanism emerged in the adapted tetraploid HAP1 cells. Despite no drastic changes in the number of aneuploid genes, tetraploid HAP1s exhibited significantly higher fitness by the end of their adaptation to continuous CIN.

Given that increased ploidy reduces the impact of expression imbalances - where gaining an extra chromosome copy decreases the imbalance ratio, for example, from one-third in diploids (trisomies) to one-fifth in tetraploids (pentasomies), and losing one chromosome copy reduces the ratio from one-half in diploids (monosomies) to one-quarter in tetraploids (trisomies) (Klockner & Campbell, 2024) - we focused our analysis on single or double chromosome losses in adapted tetraploid HAP1s and their impact on adaptation to reversine.

4.2.1 Tetraploid CIN-adapted HAP1s acquire double losses of 13q over time.

In CIN-adaptation of diploid cell lines, Adell and Klockner identified the loss of chromosome arms 13q and 6p as frequently selected aneuploidies in dipHAP1 and RPE1, respectively. Using CRISPR-Cas9, they could further dissect the importance of these chromosome arm losses and found two genes responsible for mitotic delay (CDC16 and p31comet) and reversine resistance (**see Figure 10a** (Adell et al., 2023)). In our analysis of the most common chromosome losses in tetraploid cells (**see Supplement Fig. 2**), I observed that both adapted tetHAP1s and tetRPE1 showed selection for double chromosome gains (or higher). However, the only instance of double chromosome loss (disomy) occurred in the context of 13q loss in tetHAP1s **(Figure 10b)**. As previously highlighted, tetraploidy reduces the impact of single chromosome changes, particularly losses (Baker, Lai, et al., 2024; Dewhurst et al., 2014; Klockner & Campbell, 2024). Consequently, there is no strong correlation between double 13q loss and improved growth of tetraploids under reversine. Nevertheless, we decided to investigate the effects of single and double chromosome losses by engineering 13q and 6p chromosome losses, similar to the approach taken previously in diploid cells (Adell et al., 2023)

4.3 Engineered individual chromosome deletions in tetraploid background result in the formation of additional changes but can still recapitulate reversine resistance

Klockner developed the approach of introducing chromosome arm deletions in diploid cell lines, which was refined to minimize off-target effects (Adell et al., 2023). Consequently, the same methodology was applied to engineer chromosome arm losses in tetraploid cells. However, the inherent instability of tetraploidy made off-targets and spontaneous aneuploidies nearly unavoidable during this process, indicating the need for further optimization of our protocol to engineer chromosome losses in tetraploid wild types effectively. Despite these unintended aneuploidies, we demonstrated that tetraploids with double losses of either 13q or 6p exhibit a greater degree of CIN rescue compared to those with single losses of the corresponding chromosome arms **(Figure 11)**. However, we cannot entirely attribute the reversine-rescue phenotype to the specific aneuploidies present, as clean chromosome losses are essential for more definitive conclusions. Nevertheless, our experiments highlight the role of tetraploid cells in cancer heterogeneity, as their increased tolerance to aneuploidy allows them to better adapt to various stressors during tumor progression (Vittoria et al., 2023).

To further validate the impact of single vs double chromosome 13q or 6p loss on the adaptation of engineered tetraploid HAP1 cell lines, it would be useful to conduct competition assays in the same way as in engineered diploid cells (**see Figure 5, Figure 10**). By introducing different fluorophores to the engineered tetraploids, we would be able to track fitness differences between cell lines with single vs double chromosome loss.

4.4 Tetraploidy slows down fine-tuning of karyotype refinement in response to long-term MPS1 inhibition.

Adell and Klockner showed a high correlation of chromosome gains from reversine-adapted cell lines and different cancer types. Gains of chromosomes 8, 20, and 1q were

the most prominent ones in both (Adell et al., 2023). All three chromosome gains are known to be one of the cancer's most frequent genomic alterations (Klockner & Campbell, 2024). Here, gains of chromosomes 8 and 20 are indeed present in both HAP1s and RPE1s across all ploidy states. Interestingly, multiple gains of chromosome 8 were selected only in tetraploid HAP1s, not tetraploid RPE1s. This points toward cell type-specific adaptation response. Selection of chromosome 1q gain is also different in tetraploid HAP1s than in diploids and haploids. Namely, in lower ploidy states, 1q gain is prominent early on, while in tetraploids, only at 90 days of adaptation, there is a stronger selection of 1q gain than for whole chromosome 1 gain **(supplemental fig. 2)**. The same pattern was true for the selection of double losses of 13q, as discussed above **(4.2.1)** **(Figure 10)**. These findings indicate that tetraploid cells require more time to develop more effective fine-tuning of karyotype refinement in response to induced chromosomal instability. This is, again, probably due to the generally higher tolerance of aneuploidy in tetraploid cells (Dewhurst et al., 2014).

4.5 Outlook and significance

In this thesis, I investigated the role of ploidy in complex karyotype formation and its impact on cellular adaptation to chromosomal instability. By analyzing the adaptation of haploid, diploid, and tetraploid HAP1 and RPE1 cell lines to the CIN-inducing drug reversine, we elucidated the differential mechanisms of aneuploidy selection and refinement based on ploidy state. While higher ploidy allows for faster formation of complex karyotypes, the refinement of these complex karyotypes requires longer adaptation than in lower ploidy states. A previous significant finding from a longitudinal reversine adaptation study includes the identification of a positive selection of 13q and 6p chromosome losses, which are crucial for reversine resistance in diploid-adapted HAP1 and RPE1 cells (Adell et al., 2023). The use of CRISPR/Cas9 in this report enabled targeted deletions of 13q and 6p chromosome arm, demonstrating how engineered aneuploidies can impact growth dynamics and fitness in tetraploid backgrounds despite many off-target aneuploidies. This research contributes to a deeper understanding of the

mechanisms by which aneuploidy facilitates cancer progression and heterogeneity. The increased tolerance to aneuploidy observed in tetraploid cells highlights their role as evolutionary stepping stones in the development of complex karyotypes, which often promote tumorigenesis (Dewhurst et al., 2014; Prasad et al., 2022; Vittoria et al., 2023).

Moreover, the differences in complexity of karyotype alterations across ploidies further exemplifies the evolutionary adaptability of cancer cells (Lau & Poon, 2023; Vittoria et al., 2023). Understanding this adaptability is crucial for developing strategies to counteract tumor evolution and resistance mechanisms. However, from this study, performing RNA-seq analysis and comparing the transcriptome profiles across ploidy states would be useful. By analyzing the differences in transcriptional gene expression, we could unravel unique features in reversine-adapted tetraploid cells not found in diploid or haploid backgrounds. A proteomic analysis could further follow this to reveal differences in post-transcriptional and post-translational modifications across ploidies (Chang et al., 2024). This would help us further understand the consequences of adaptation through aneuploidy in different ploidy states.

Ultimately, this work underscores the importance of studying chromosomal alterations in cancer as it sheds light on basic biological principles of complex karyotype formation.

5. References

Adell, M. A. Y., Klockner, T. C., Hofler, R., Wallner, L., Schmid, J., Markovic, A., Martyniak, A., & Campbell, C. S. (2023). Adaptation to spindle assembly checkpoint inhibition through the selection of specific aneuploidies. *Genes Dev*, *37*(5-6), 171-190. https://doi.org/10.1101/gad.350182.122

Andrade, J. R., Gallagher, A. D., Maharaj, J., & McClelland, S. E. (2023). Disentangling the roles of aneuploidy, chromosomal instability and tumour heterogeneity in developing resistance to cancer therapies. *Chromosome Res*, *31*(4), 28. https://doi.org/10.1007/s10577-023-09737-5

Baker, T. M., Lai, S., Lynch, A. R., Lesluyes, T., Yan, H., Ogilvie, H. A., Verfaillie, A., Dentro, S., Bowes, A. L., Pillay, N., Flanagan, A. M., Swanton, C., Spellman, P. T., Tarabichi, M., & Van Loo, P. (2024). The history of chromosomal instability in genome doubled tumors. *Cancer Discov*. https://doi.org/10.1158/2159-8290.CD-23-1249

Baker, T. M., Waise, S., Tarabichi, M., & Van Loo, P. (2024). Aneuploidy and complex genomic rearrangements in cancer evolution. *Nat Cancer*. https://doi.org/10.1038/s43018-023-00711-y

Bakhoum, S. F., Ngo, B., Laughney, A. M., Cavallo, J. A., Murphy, C. J., Ly, P., Shah, P., Sriram, R. K., Watkins, T. B. K., Taunk, N. K., Duran, M., Pauli, C., Shaw, C., Chadalavada, K., Rajasekhar, V. K., Genovese, G., Venkatesan, S., Birkbak, N. J., McGranahan, N., . . . Cantley, L. C. (2018). Chromosomal instability drives metastasis through a cytosolic DNA response. *Nature*, *553*(7689), 467-472. https://doi.org/10.1038/nature25432

Baudoin, N. C., & Bloomfield, M. (2021). Karyotype Aberrations in Action: The Evolution of Cancer Genomes and the Tumor Microenvironment. *Genes (Basel)*, *12*(4). https://doi.org/10.3390/genes12040558

Beach, R. R., Ricci-Tam, C., Brennan, C. M., Moomau, C. A., Hsu, P. H., Hua, B., Silberman, R. E., Springer, M., & Amon, A. (2017). Aneuploidy Causes Non-genetic Individuality. *Cell*, *169*(2), 229-242 e221. https://doi.org/10.1016/j.cell.2017.03.021

Ben-David, U., & Amon, A. (2020). Context is everything: aneuploidy in cancer. *Nature Reviews Genetics*, *21*(1), 44-62. https://doi.org/10.1038/s41576-019-0171-x

Beroukhim, R., Mermel, C. H., Porter, D., Wei, G., Raychaudhuri, S., Donovan, J., Barretina, J., Boehm, J. S., Dobson, J., Urashima, M., Mc Henry, K. T., Pinchback, R. M., Ligon, A. H., Cho, Y. J., Haery, L., Greulich, H., Reich, M., Winckler, W., Lawrence, M. S., . . . Meyerson, M. (2010). The landscape of somatic copy-number alteration across human cancers. *Nature*, *463*(7283), 899-905. https://doi.org/10.1038/nature08822

Bielski, C. M., Zehir, A., Penson, A. V., Donoghue, M. T. A., Chatila, W., Armenia, J., Chang, M. T., Schram, A. M., Jonsson, P., Bandlamudi, C., Razavi, P., Iyer, G., Robson, M. E., Stadler, Z. K., Schultz, N., Baselga, J., Solit, D. B., Hyman, D. M., Berger, M. F., & Taylor, B. S. (2018). Genome doubling shapes the evolution and prognosis of advanced cancers. *Nat Genet*, *50*(8), 1189-1195. https://doi.org/10.1038/s41588-018-0165-1

Bigner, S. H., Mark, J., & Bigner, D. D. (1990). Cytogenetics of human brain tumors. *Cancer Genet Cytogenet*, *47*(2), 141-154. https://doi.org/10.1016/0165-4608(90)90024-5

Bochtler, T., Kartal-Kaess, M., Granzow, M., Hielscher, T., Cosenza, M. R., Herold-Mende, C., Jauch, A., & Kramer, A. (2019). Micronucleus formation in human cancer cells is biased by chromosome size. *Genes Chromosomes Cancer*, *58*(6), 392-395. https://doi.org/10.1002/gcc.22707

Burkard, M. E., & Weaver, B. A. (2017). Tuning Chromosomal Instability to Optimize Tumor Fitness. *Cancer Discov*, *7*(2), 134-136. https://doi.org/10.1158/2159-8290.CD-16-1415

Burrell, R. A., McGranahan, N., Bartek, J., & Swanton, C. (2013). The causes and consequences of genetic heterogeneity in cancer evolution. *Nature*, *501*(7467), 338-345. https://doi.org/10.1038/nature12625

Chang, E., Kim, S. J., Hwang, H. S., Song, K. J., Kim, K., Kim, M. S., Jang, S. J., You, S., Kim, K. P., & An, J. Y. (2024). Pan-cancer proteogenomic landscape of whole-genome doubling reveals putative therapeutic targets in various cancer types. *Clin Transl Med*, *14*(8), e1796. https://doi.org/10.1002/ctm2.1796

Cheeseman, I. M. (2014). The kinetochore. *Cold Spring Harb Perspect Biol*, *6*(7), a015826. https://doi.org/10.1101/cshperspect.a015826

Cohen, J. (2002). Sorting out chromosome errors. *Science*, *296*(5576), 2164-2166. https://doi.org/10.1126/science.296.5576.2164

Davoli, T., & de Lange, T. (2012). Telomere-driven tetraploidization occurs in human cells undergoing crisis and promotes transformation of mouse cells. *Cancer Cell*, *21*(6), 765-776. https://doi.org/10.1016/j.ccr.2012.03.044

Devon A. Lukow1, a. J. M. S. (2022). Chromosomal instability and aneuploidy as

causes of cancer drug resistance [Review Article]. *Trends in Cancer*, *8*, 11. https://doi.org/https://doi.org/10.1016/j.trecan.2021.09.002

Dewhurst, S. M., McGranahan, N., Burrell, R. A., Rowan, A. J., Gronroos, E., Endesfelder, D., Joshi, T., Mouradov, D., Gibbs, P., Ward, R. L., Hawkins, N. J., Szallasi, Z., Sieber, O. M., & Swanton, C. (2014). Tolerance of whole-genome doubling propagates chromosomal instability and accelerates cancer genome evolution. *Cancer Discov*, *4*(2), 175-185. https://doi.org/10.1158/2159-8290.CD-13-0285

Donne, R., Saroul-Ainama, M., Cordier, P., Celton-Morizur, S., & Desdouets, C. (2020). Polyploidy in liver development, homeostasis and disease. *Nat Rev Gastroenterol Hepatol*, *17*(7), 391-405. https://doi.org/10.1038/s41575-020-0284-x

Duelli, D. M., Padilla-Nash, H. M., Berman, D., Murphy, K. M., Ried, T., & Lazebnik, Y. (2007). A virus causes cancer by inducing massive chromosomal instability through cell fusion. *Curr Biol*, *17*(5), 431-437. https://doi.org/10.1016/j.cub.2007.01.049

Duncan, A. W. (2013). Aneuploidy, polyploidy and ploidy reversal in the liver. *Semin Cell Dev Biol*, *24*(4), 347-356. https://doi.org/10.1016/j.semcdb.2013.01.003

Fujiwara, T., Bandi, M., Nitta, M., Ivanova, E. V., Bronson, R. T., & Pellman, D. (2005). Cytokinesis failure generating tetraploids promotes tumorigenesis in p53-null cells. *Nature*, *437*(7061), 1043-1047. https://doi.org/10.1038/nature04217

Ganem, N. J., Storchova, Z., & Pellman, D. (2007). Tetraploidy, aneuploidy and cancer. *Curr Opin Genet Dev*, *17*(2), 157-162. https://doi.org/10.1016/j.gde.2007.02.011

Hassold, T., & Hunt, P. (2001). To err (meiotically) is human: the genesis of human aneuploidy. *Nat Rev Genet*, *2*(4), 280-291. https://doi.org/10.1038/35066065

Ichijima, Y., Yoshioka, K., Yoshioka, Y., Shinohe, K., Fujimori, H., Unno, J., Takagi, M., Goto, H., Inagaki, M., Mizutani, S., & Teraoka, H. (2010). DNA lesions induced by replication stress trigger mitotic

aberration and tetraploidy development. *PLoS One*, *5*(1), e8821. https://doi.org/10.1371/journal.pone.0008821

Ippolito, M. R., Martis, V., Martin, S., Tijhuis, A. E., Hong, C., Wardenaar, R., Dumont, M., Zerbib, J., Spierings, D. C. J., Fachinetti, D., Ben-David, U., Foijer, F., & Santaguida, S. (2021). Gene copy-number changes and chromosomal instability induced by aneuploidy confer resistance to chemotherapy. *Developmental Cell*, *56*(17), 2440-2454.e2446. https://doi.org/10.1016/j.devcel.2021.07.006

Klockner, T. C., & Campbell, C. S. (2024). Selection forces underlying aneuploidy patterns in cancer. *Mol Cell Oncol*, *11*(1), 2369388. https://doi.org/10.1080/23723556.2024.2369388

Kuznetsova, A. Y., Seget, K., Moeller, G. K., de Pagter, M. S., de Roos, J. A., Durrbaum, M., Kuffer, C., Muller, S., Zaman, G. J., Kloosterman, W. P., & Storchova, Z. (2015). Chromosomal instability, tolerance of mitotic errors and multidrug resistance are promoted by tetraploidization in human cells. *Cell Cycle*, *14*(17), 2810-2820. https://doi.org/10.1080/15384101.2015.1068482

Lara-Gonzalez, P., Pines, J., & Desai, A. (2021). Spindle assembly checkpoint activation and silencing at kinetochores. *Semin Cell Dev Biol*, *117*, 86-98. https://doi.org/10.1016/j.semcdb.2021.06.009

Lau, T. Y., & Poon, R. Y. C. (2023). Whole-Genome Duplication and Genome Instability in Cancer Cells: Double the Trouble. *Int J Mol Sci*, *24*(4). https://doi.org/10.3390/ijms24043733

Laughney, A. M., Elizalde, S., Genovese, G., & Bakhoum, S. F. (2015). Dynamics of Tumor Heterogeneity Derived from Clonal Karyotypic Evolution. *Cell Rep*, *12*(5), 809-820. https://doi.org/10.1016/j.celrep.2015.06.065

Lee, A. J., Endesfelder, D., Rowan, A. J., Walther, A., Birkbak, N. J., Futreal, P. A., Downward, J., Szallasi, Z., Tomlinson, I. P., Howell, M., Kschischo, M., & Swanton, C. (2011). Chromosomal instability confers intrinsic multidrug resistance. *Cancer Res*, *71*(5), 1858-1870. https://doi.org/10.1158/0008-5472.CAN-10-3604

Lens, S. M. A., & Medema, R. H. (2019). Cytokinesis defects and cancer. *Nat Rev Cancer*, *19*(1), 32-45. https://doi.org/10.1038/s41568-018-0084-6

Lopez, S., Lim, E. L., Horswell, S., Haase, K., Huebner, A., Dietzen, M., Mourikis, T. P., Watkins, T. B. K., Rowan, A., Dewhurst, S. M., Birkbak, N. J., Wilson, G. A., Van Loo, P., Jamal-Hanjani, M., Consortium, T. R., Swanton, C., & McGranahan, N. (2020). Interplay between whole-genome doubling and the accumulation of deleterious alterations in cancer evolution. *Nat Genet*, *52*(3), 283-293. https://doi.org/10.1038/s41588-020-0584-7

Lukow, D. A., Sausville, E. L., Suri, P., Chunduri, N. K., Wieland, A., Leu, J., Smith, J. C., Girish, V., Kumar, A. A., Kendall, J., Wang, Z., Storchova, Z., & Sheltzer, J. M. (2021). Chromosomal instability accelerates the evolution of resistance to anti-cancer therapies. *Dev Cell*, *56*(17), 2427-2439 e2424. https://doi.org/10.1016/j.devcel.2021.07.009

Maiato, H., & Silva, S. (2023). Double-checking chromosome segregation. *J Cell Biol*, *222*(5). https://doi.org/10.1083/jcb.202301106

Mazzi, S., Lordier, L., Debili, N., Raslova, H., & Vainchenker, W. (2018). Megakaryocyte and polyploidization. *Exp Hematol*, *57*, 1-13. https://doi.org/10.1016/j.exphem.2017.10.001

McAinsh, A. D., & Kops, G. (2023). Principles and dynamics of spindle assembly checkpoint signalling. *Nat Rev Mol Cell Biol*, *24*(8), 543-559. https://doi.org/10.1038/s41580-023-00593-z

Mora-Bermudez, F., Kanis, P., Macak, D., Peters, J., Naumann, R., Xing, L., Sarov, M., Winkler, S., Oegema, C. E., Haffner, C., Wimberger, P., Riesenberg, S., Maricic, T., Huttner, W. B., & Paabo, S. (2022). Longer metaphase and fewer chromosome segregation errors in modern human than Neanderthal brain development. *Sci Adv*, *8*(30), eabn7702. https://doi.org/10.1126/sciadv.abn7702

Nguyen, H. G., Makitalo, M., Yang, D., Chinnappan, D., St Hilaire, C., & Ravid, K. (2009). Deregulated Aurora-B induced tetraploidy promotes tumorigenesis. *FASEB J*, *23*(8), 2741-2748. https://doi.org/10.1096/fj.09-130963

Oromendia, A. B., Dodgson, S. E., & Amon, A. (2012). Aneuploidy causes proteotoxic stress in yeast. *Genes Dev*, *26*(24), 2696-2708. https://doi.org/10.1101/gad.207407.112

Passerini, V., Ozeri-Galai, E., de Pagter, M. S., Donnelly, N., Schmalbrock, S., Kloosterman, W. P., Kerem, B., & Storchova, Z. (2016). The presence of extra chromosomes leads to genomic instability. *Nat Commun*, *7*, 10754. https://doi.org/10.1038/ncomms10754

Peterson, N. G., & Fox, D. T. (2021). Communal living: the role of polyploidy and syncytia in tissue biology. *Chromosome Res*, *29*(3-4), 245-260. https://doi.org/10.1007/s10577-021-09664-3

Prasad, K., Bloomfield, M., Levi, H., Keuper, K., Bernhard, S. V., Baudoin, N. C., Leor, G., Eliezer, Y., Giam, M., Wong, C. K., Rancati, G., Storchova, Z., Cimini, D., & Ben-David, U. (2022). Whole-Genome Duplication Shapes the Aneuploidy Landscape of Human Cancers. *Cancer Res*, *82*(9), 1736-1752. https://doi.org/10.1158/0008-5472.CAN-21-2065

Quinton, R. J., DiDomizio, A., Vittoria, M. A., Kotynkova, K., Ticas, C. J., Patel, S., Koga, Y., Vakhshoorzadeh, J., Hermance, N., Kuroda, T. S., Parulekar, N., Taylor, A. M., Manning, A. L., Campbell, J. D., & Ganem, N. J. (2021). Publisher Correction: Whole-genome doubling confers unique genetic vulnerabilities on tumour cells. *Nature*, *593*(7860), E15. https://doi.org/10.1038/s41586-021-03591-3

Ravichandran, M. C., Fink, S., Clarke, M. N., Hofer, F. C., & Campbell, C. S. (2018). Genetic interactions between specific chromosome copy number alterations dictate complex aneuploidy patterns. *Genes Dev*, *32*(23-24), 1485-1498. https://doi.org/10.1101/gad.319400.118

Sansregret, L., Vanhaesebroeck, B., & Swanton, C. (2018). Determinants and clinical implications of chromosomal instability in cancer. *Nat Rev Clin Oncol*, *15*(3), 139-150. https://doi.org/10.1038/nrclinonc.2017.198

Santaguida, S., & Amon, A. (2015). Short- and long-term effects of chromosome mis-segregation and aneuploidy. *Nat Rev Mol Cell Biol*, *16*(8), 473-485. https://doi.org/10.1038/nrm4025

Santaguida, S., Richardson, A., Iyer, D. R., M'Saad, O., Zasadil, L., Knouse, K. A., Wong, Y. L., Rhind, N., Desai, A., & Amon, A. (2017). Chromosome Mis-segregation Generates Cell-Cycle-Arrested Cells with Complex Karyotypes that Are Eliminated by the Immune System. *Dev Cell*, *41*(6), 638-651 e635. https://doi.org/10.1016/j.devcel.2017.05.022

Schrock, M. S., Stromberg, B. R., Scarberry, L., & Summers, M. K. (2020). APC/C ubiquitin ligase: Functions and mechanisms in tumorigenesis. *Semin Cancer Biol*, *67*(Pt 2), 80-91. https://doi.org/10.1016/j.semcancer.2020.03.001

Schukken, K. M., & Sheltzer, J. M. (2022). Extensive protein dosage compensation in aneuploid human cancers. *Genome Res*, *32*(7), 1254-1270. https://doi.org/10.1101/gr.276378.121

Selmecki, A. M., Maruvka, Y. E., Richmond, P. A., Guillet, M., Shoresh, N., Sorenson, A. L., De, S., Kishony, R., Michor, F., Dowell, R., & Pellman, D. (2015). Polyploidy can drive rapid adaptation in yeast. *Nature*, *519*(7543), 349-352. https://doi.org/10.1038/nature14187

Sheltzer, J. M., & Amon, A. (2011). The aneuploidy paradox: costs and benefits of an incorrect karyotype. *Trends Genet*, *27*(11), 446-453. https://doi.org/10.1016/j.tig.2011.07.003

Stingele, S., Stoehr, G., Peplowska, K., Cox, J., Mann, M., & Storchova, Z. (2012). Global analysis of genome, transcriptome and proteome reveals the response to aneuploidy in human cells. *Mol Syst Biol*, *8*, 608. https://doi.org/10.1038/msb.2012.40

Tanaka, T. U. (2005). Chromosome bi-orientation on the mitotic spindle. *Philos Trans R Soc Lond B Biol Sci*, *360*(1455), 581-589. https://doi.org/10.1098/rstb.2004.1612

Teitelbaum, S. L. (2000). Bone resorption by osteoclasts. *Science*, *289*(5484), 1504-1508. https://doi.org/10.1126/science.289.5484.1504

Tijhuis, A. E., Johnson, S. C., & McClelland, S. E. (2019). The emerging links between chromosomal instability (CIN), metastasis, inflammation and tumour immunity. *Mol Cytogenet*, *12*, 17. https://doi.org/10.1186/s13039-019-0429-1

Torres, E. M., Sokolsky, T., Tucker, C. M., Chan, L. Y., Boselli, M., Dunham, M. J., & Amon, A. (2007). Effects of aneuploidy on cellular physiology and cell division in haploid yeast. *Science*, *317*(5840), 916-924. https://doi.org/10.1126/science.1142210

Umbreit, N. T., Zhang, C. Z., Lynch, L. D., Blaine, L. J., Cheng, A. M., Tourdot, R., Sun, L., Almubarak, H. F., Judge, K., Mitchell, T. J., Spektor, A., & Pellman, D. (2020). Mechanisms generating cancer genome complexity from a single cell division error. *Science*, *368*(6488). https://doi.org/10.1126/science.aba0712

van Dijk, E., van den Bosch, T., Lenos, K. J., El Makrini, K., Nijman, L. E., van Essen, H. F. B., Lansu, N., Boekhout, M., Hageman, J. H., Fitzgerald, R. C., Punt, C. J. A., Tuynman, J. B., Snippert, H. J. G., Kops, G., Medema, J. P., Ylstra, B., Vermeulen, L., & Miedema, D. M. (2021). Chromosomal copy number heterogeneity predicts survival rates across cancers. *Nat Commun*, *12*(1), 3188. https://doi.org/10.1038/s41467-021-23384-6

Vendramin, R., Litchfield, K., & Swanton, C. (2021). Cancer evolution: Darwin and beyond. *EMBO J*, *40*(18), e108389. https://doi.org/10.15252/embj.2021108389

Vitale, I., Galluzzi, L., Senovilla, L., Criollo, A., Jemaa, M., Castedo, M., & Kroemer, G. (2011). Illicit survival of cancer cells during polyploidization and depolyploidization. *Cell Death Differ*, *18*(9), 1403-1413. https://doi.org/10.1038/cdd.2010.145

Vittoria, M. A., Quinton, R. J., & Ganem, N. J. (2023). Whole-genome doubling in tissues and tumors. *Trends Genet*, *39*(12), 954-967. https://doi.org/10.1016/j.tig.2023.08.004

Wang, Y., & Tamori, Y. (2024). Polyploid Cancer Cell Models in Drosophila. *Genes (Basel)*, *15*(1). https://doi.org/10.3390/genes15010096

Wartosch, L., Schindler, K., Schuh, M., Gruhn, J. R., Hoffmann, E. R., McCoy, R. C., & Xing, J. (2021). Origins and mechanisms leading to aneuploidy in human eggs. *Prenat Diagn*, *41*(5), 620-630. https://doi.org/10.1002/pd.5927

Watkins, T. B. K., Lim, E. L., Petkovic, M., Elizalde, S., Birkbak, N. J., Wilson, G. A., Moore, D. A., Gronroos, E., Rowan, A., Dewhurst, S. M., Demeulemeester, J., Dentro, S. C., Horswell, S., Au, L., Haase, K., Escudero, M., Rosenthal, R., Bakir, M. A., Xu, H., . . . Swanton, C. (2020). Pervasive chromosomal

instability and karyotype order in tumour evolution. *Nature*, *587*(7832), 126-132. https://doi.org/10.1038/s41586-020-2698-6

Weaver, B. A., & Cleveland, D. W. (2008). The aneuploidy paradox in cell growth and tumorigenesis. *Cancer Cell*, *14*(6), 431-433. https://doi.org/10.1016/j.ccr.2008.11.011

Williams, B. R., Prabhu, V. R., Hunter, K. E., Glazier, C. M., Whittaker, C. A., Housman, D. E., & Amon, A. (2008). Aneuploidy affects proliferation and spontaneous immortalization in mammalian cells. *Science*, *322*(5902), 703-709. https://doi.org/10.1126/science.1160058

Zack, T. I., Schumacher, S. E., Carter, S. L., Cherniack, A. D., Saksena, G., Tabak, B., Lawrence, M. S., Zhsng, C. Z., Wala, J., Mermel, C. H., Sougnez, C., Gabriel, S. B., Hernandez, B., Shen, H., Laird, P. W., Getz, G., Meyerson, M., & Beroukhim, R. (2013). Pan-cancer patterns of somatic copy number alteration. *Nat Genet*, *45*(10), 1134-1140. https://doi.org/10.1038/ng.2760

Zhang, S., Zhou, K., Luo, X., Li, L., Tu, H. C., Sehgal, A., Nguyen, L. H., Zhang, Y., Gopal, P., Tarlow, B. D., Siegwart, D. J., & Zhu, H. (2018). The Polyploid State Plays a Tumor-Suppressive Role in the Liver. *Dev Cell*, *47*(3), 390. https://doi.org/10.1016/j.devcel.2018.10.020

Zhang, Y., Young, R., Garvanska, D. H., Song, C., Zhai, Y., Wang, Y., Jiang, H., Fang, J., Nilsson, J., Alfieri, C., & Zhang, G. (2024). Functional analysis of Cdc20 reveals a critical role of CRY box in mitotic checkpoint signaling. *Commun Biol*, *7*(1), 164. https://doi.org/10.1038/s42003-024-05859-6

6. Supplement

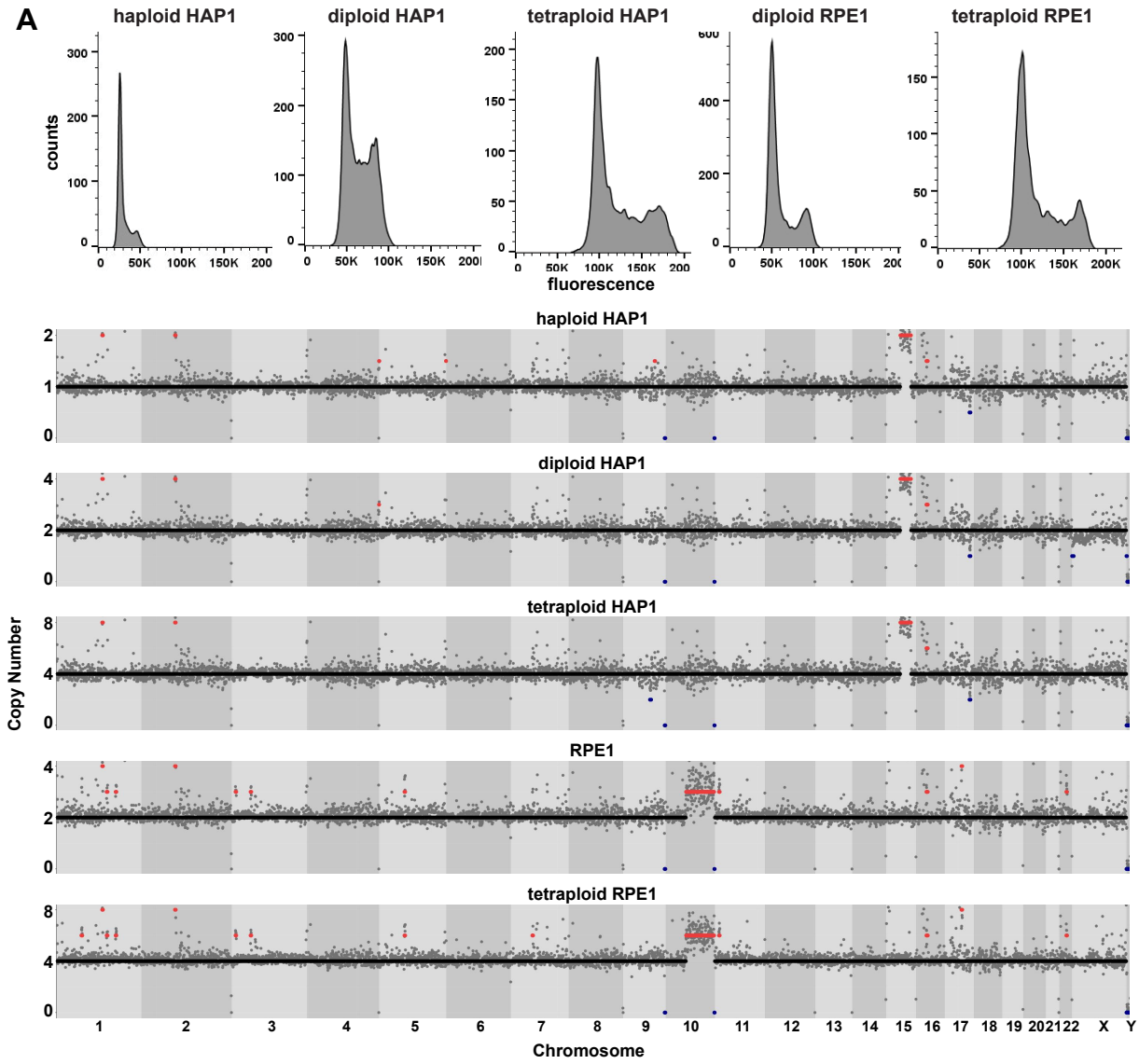

Supplemental Figure 1. Cell lines used for determining the affect of ploidy on adaptation to CIN. a) Plots of DNA contents of 5 cell lines. b) Gingko profiles showing chromosome copy numbers of 5 cell lines. Three HAP1 and two RPE1 cell lines that differ only in their ploidy have been engineered by cytokinesis inhibition. Unpublished data are from Manuel Alonso y Adell.

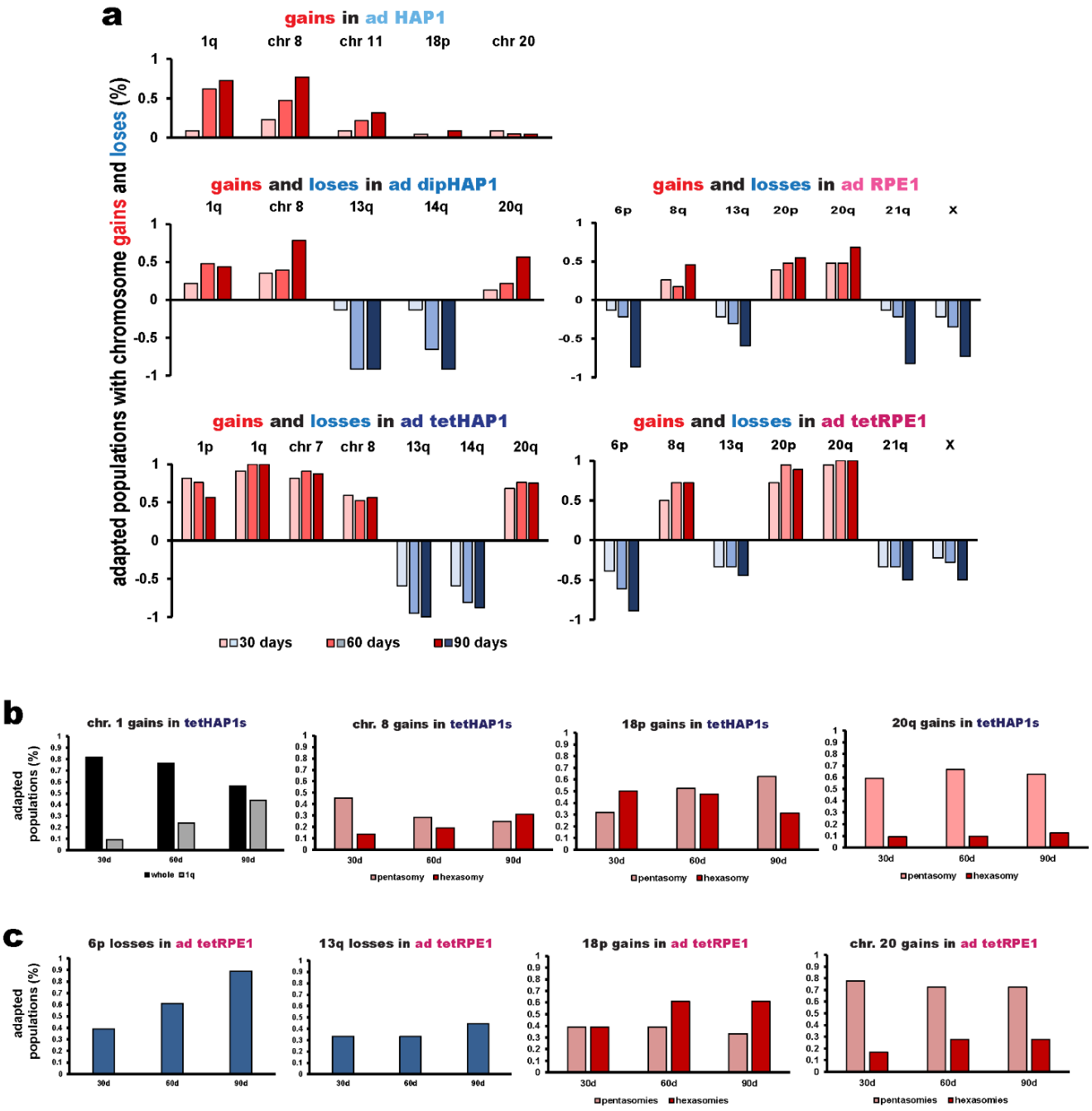

Supplemental Figure 2: Analysis of most prominent chromosome gains and loses. (a) The percentage of adapted cell lines with most common chromosome arm copy number changes in all 5 adapted cell lines at 30, 60 and 90 days of reversine adaptation. (b) The percentage of adapted cell lines with specific aneuploidies in tetraploid HAP1s. (c) The percentage of adapted cell lines with specific aneuploidies in tetraploid RPE1s. (d) Relative proportion of types of copy number changes of the reversine-adapted cell populations at 30, 60 and 90 days from each cell line for acrocentric chromosomes considered as chromosome arms.

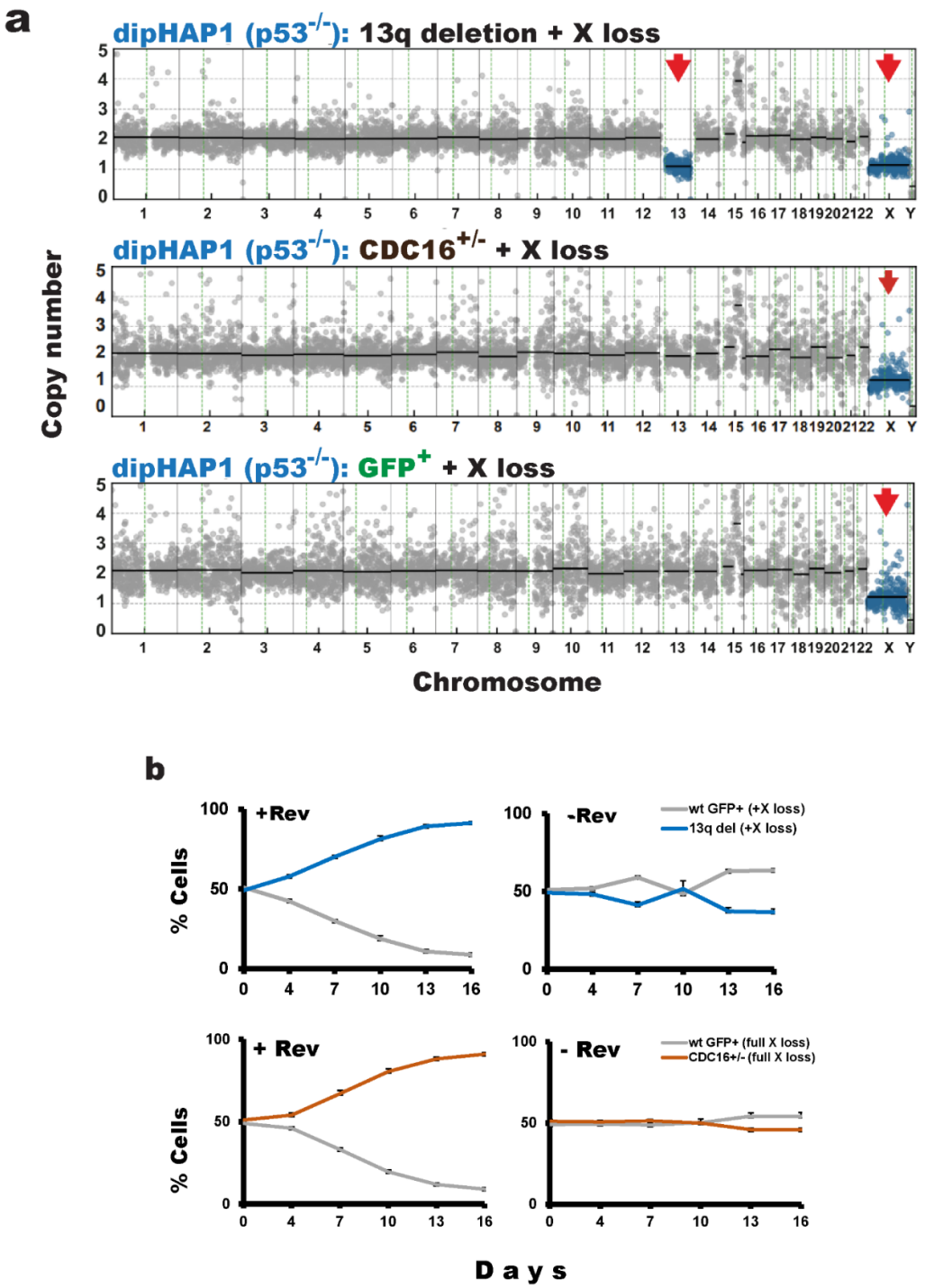

Supplemental Figure 3. Cell lines used for the competition assays. (a) Chromosome copy number profiles of the cell lines used for the co-cultivation assays. (b) Second independent co-cultivations of the: upper graphs → 13g + X loss cell line and the X loss-GFP cell line. Lower graphs → CDC16+/- + X loss cell line and the X loss GFP cell line. The mean +/- SD for 6 separate populations of cells in one time course are shown.

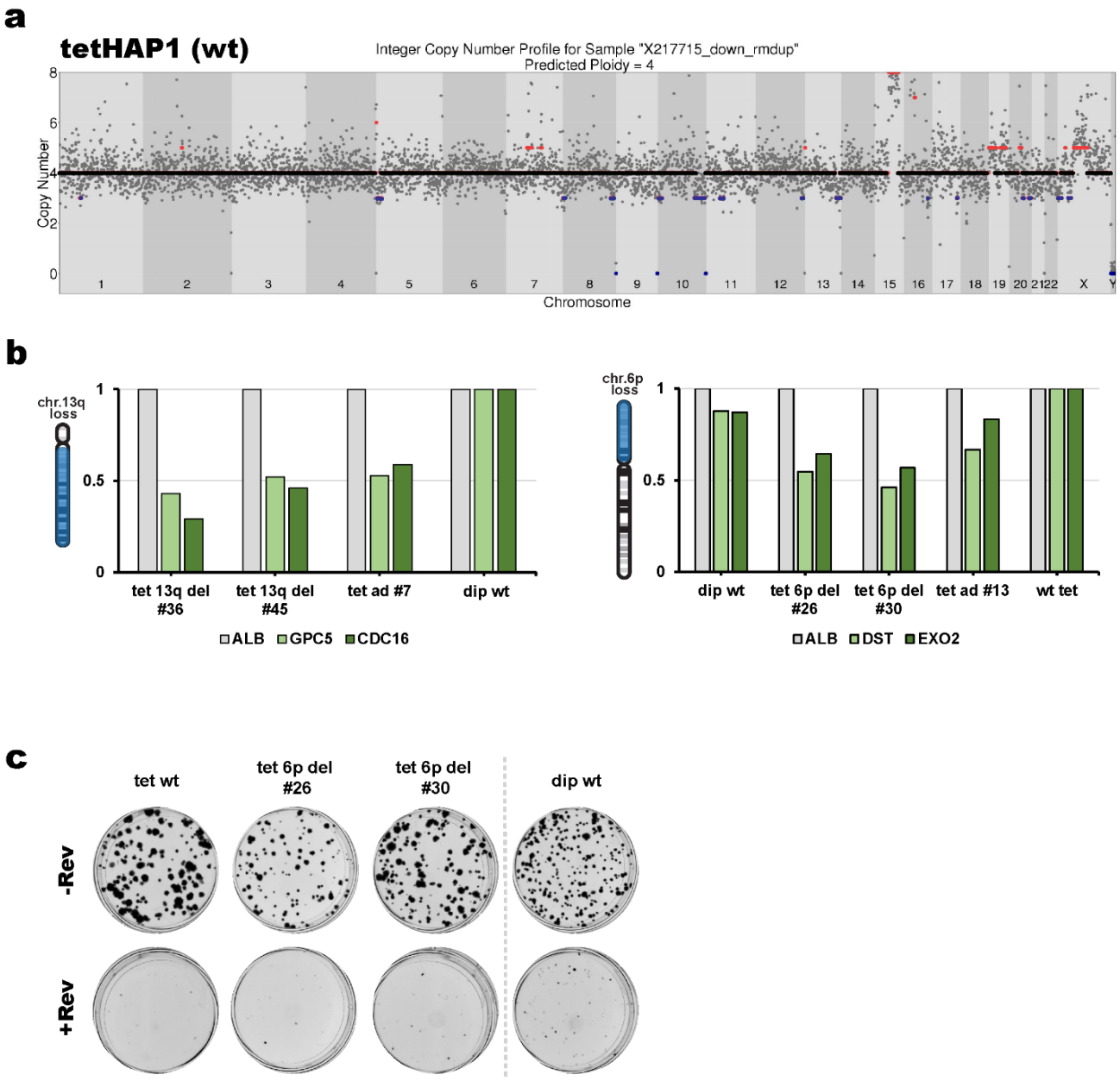

Supplemental Figure 4: Engineering chromosome losses in tetraploid HAP1s. (a) Chromosome copy number profile of the cell line used for the engineering chromosome deletions. (b) qPCR results of the engineered 13q or 6p loss in tetraploid cell line measured after all CFAs were performed. Values are firstly normalized to reference gene albumin (ALB – on chr 4) and then to tetraploid wt GPC5 and CDC16 values (both on chromosome 13q (see Methods). (c) Colony formation assay results for 6p deletion, upper row shows cells grown under normal conditions, lower row shows cells grown under reversine.

7 List of figures

8 List of supplemental figures

9 List of tables

Supplemental Table 2. List of parental and engineered cell lines used in this project and their karyotypic deviations.

Supplemental Table 3. List of media, supplements, and buffers.

Supplemental Table 4. List of plasmids used for lentiviral transduction

Supplemental Table 5. sgRNAs used for engineering whole chromosome arm deletions.

Supplemental Table 6. Primers used for qPCR screening of chromosome arm deletions.

Supplemental Table 7. List of reagents and equipment

Supplemental Table 8. Sequences of primers used for qPCR screening for identification of chromosome deletions. See primer binding sites in Figure 6.

Supplemental Table 1. List of parental cell lines used in this project.

Cell line	Tissue	Phenotype	Sex	Culture Medium	Source
HAP1 TP53 KO	Chronic myeloid leukemia (CML)	Adherent	Male	IMDM (Sigma-Aldrich)	Campbell Lab
Diploid HAP1 (dipHAP1) TP53 KO	Chronic myeloid leukemia (CML)	Adherent	Male	IMDM (Sigma-Aldrich)	Campbell Lab Obtained by single sorting for diploids from parental haploid population
Tetraploid HAP1 (tetHAP1)	Chronic myeloid leukemia (CML)	Adherent	Male	IMDM (Sigma-Aldrich)	Campbell Lab

TP53 KO					Obtained by tetraploidization of diploids
RPE1 TP53 KO	Retina epithelial	Adherent	Female	DMEM (Sigma-Aldrich) + 2 mmol L-Glutamine (Gibco) + 1mM NatriumPyruvate (Sigma-Aldrich)	Campbell Lab
Tetraploid RPE1 TP53 KO	Retina epithelial	Adherent	Female	DMEM (Sigma-Aldrich) + 2 mmol L-Glutamine (Gibco) + 1mM NatriumPyruvate (Sigma-Aldrich)	Campbell Lab Obtained by tetraploidization of diploids

- 10% FBS and 1% Penicillin-Streptomycin were added in both, IMDM and DMEM culture media.

Supplemental Table 2. List of parental and engineered cell lines used in this project and their karyotypic deviations.

Cell line	Karyotype deviations from euploidy
HAP1 TP53 KO	Segmental chr. 15q gain
dipHAP1 TP53 KO	Segmental chr. 15q gain
dipHAP1 TP53 KO GFP^{+}	Segmental chr. 15q gain; Full chromosome X loss

tetHAP1 TP53 KO	Segmental chr. 15q gain
tetHAP1 TP53 KO GFP^{+}	Segmental chr. 15q gain; Full chromosome X loss (disomy)
RPE1 TP53 KO	Segmental chr. 10q gain
tetRPE1 TP53 KO	Segmental chr. 10q gain
tetHAP1 TP53 KO 13q del #36	Segmental chr. 15q gain; 1q loss; 7q loss; 13q loss;
tetHAP1 TP53 KO 13q del #45	Segmental chr. 15q gain; 8q gain; 13q loss; 16 loss; X loss
tetHAP1 TP53 KO 6p del #26	Segmental chr. 15q gain; 4p loss; 6p loss; 7q loss; 12p loss;
tetHAP1 TP53 KO 6p del #30	Segmental chr. 15q gain

Supplemental Table 3. List of media, supplements, and buffers.

Name	**Company**	**Notes**
IMDM	Sigma-Aldrich	**For growing cells**: always supplemented with 10% PBS and 1% FBS **For freezing cells**: non-supplemented IMDM is mixed with 1% PBS and 0.9% DMSO

DMEM	Sigma-Aldrich	
L-Glutamine	Gibco	2 mmol
Natrium Pyruvate	Sigma-Aldrich	1 mM
Penicillin-Streptomycin		1x
FBS		
BSA	Sigma-Aldrich	
PBS		
Trypsin	Sigma-Aldrich	
DMSO		
FuGENE HD	Promega	
XtremeGene 9	Roche	

Supplemental Table 4. List of plasmids used for lentiviral transduction.

Name	**Addgene ID**
Envelope (pMD2.G)	#12259
Packaging (psPAX2)	#12260
copGFP	

Supplemental Table 5. sgRNAs used for engineering whole chromosome arm deletions.

Name	Sequence	Reference
Deletion of chromosome arm 6p		
sgRNA 6p A	ACGGTTTCATTAGTCATACC	Adell and Klockner, 2023
Deletion of chromosome arm 13q		
sgRNA 13q A	GGGGGAGTGAATGTGAGTGA	Adell and Klockner, 2023

Supplemental Table 6. Primers used for qPCR screening of chromosome arm deletions.

Name	Sequence	Reference
Deletion of chromosome arm 6p		
sgRNA 6p A	ACGGTTTCATTAGTCATACC	Adell and Klockner, 2023
Deletion of chromosome arm 13q		
sgRNA 13q A	GGGGGAGTGAATGTGAGTGA	Adell and Klockner, 2023

Reagents and equipment

Supplemental Table 7. List of reagents and equipment

Name	Company	Notes
5x Phusion HF Reaction Buffer	Thermo Fisher	
Phusion High-Fidelity DNA Polymerase	Cell Signalling	
Deoxynucleotide (dNTP) Solution Mix	New England BioLabs Inc.	
Quick-Load® Purple 1 kb DNA Ladder	New England Biolabs	
Orange G	AppliChem	
Gel DocTM XR+	BIO RAD	
Luna Universal qPCR Master Mix	New England BioLabs Inc.	
Mastercycler realplex4 epgradient S	Eppendorf	
Microplate 96 well, PS, FBOTTOM, CLEAR	Greiner bio-one	
Fisherbrand TM Standard Minicentrifuge	Thermo Fisher Scientific	
EDTA	AppliChem	
Proteinase K	Sigma Aldrich	20 mg/ml
Microsoft Excel 2007	Microsoft	
GraphPad Prism 7	GraphPad Software	
Image J	National Institute of Health	

Python 3.8	for NGS data	
Agarose	GERBU	
T100TM Thermal Cycler	BIO RAD	
Sonicator Sonopuls	Bandelin	
Megafuge 1.0 R	Thermo Fischer Scientific	
PCR 8-tube strips, with separate domed cap strips	VWR	
PeqGreen	VWR	

Supplemental Table 8. Sequences of primers used for qPCR screening for identification of chromosome deletions. See primer binding sites in Figure 6.

Name		**Sequence**	**Reference**	
Chromosome 6p deletions				Adell, et al 2023
EXOC2	fw	ATGTCTCGATCACGACAACCC	PrimerBank, ID: 30581133c1	
	rev	GGCCAGTCCCCAGATTTTCT		
DST	fw	CTACCAGCACTCGAACCAGTC	PrimerBank, ID: 291290967c1	
	rev	GCCGAAGCTAATGCAAGAGTTG		
Chromosome 13q deletions				

CDC16	fw			
	rev			
GPC5	fw	GGTGTGACTGACAGTTCCCTG	PrimerBank, ID: 215272348c3	
	rev	TGCAGATAGTCTGTGGTGTTGAT		
Control primer – chromosome 4				
ALB	fw	TGTTGCATGAGAAAACGCCA	Bremer et al. 2015	
	rev	GTCGCCTGTTCAACCAAGGAT		

Abstract

Abnormal chromosome numbers, or aneuploidies, are present in more than 90% of solid tumors, with over 30% of these cancer cells being polyploid. Aneuploidy is normally detrimental but can provide certain fitness advantages in cancer cells. Higher rates of chromosome missegregation lead to chromosomal instability (CIN), which offers various karyotype complexities that can be beneficial under certain stress conditions. Polyploid cancer cells undergo higher rates of CIN, leading to greater genetic heterogeneity compared to diploid cells. Adell and Klockner (2023) tracked complex karyotype development in diploid cell lines adapted to the spindle assembly checkpoint inhibitor reversine, identifying that the selective loss of chromosomes 13q and 6p leads to reversine resistance due to genes CDC16 and p31commet located on these chromosomes (Adell et al., 2023). In parallel, A. Adell performed the same adaptation protocol on human cell lines of the haploid and tetraploid backgrounds. In this report, I examined aneuploidy patterns in haploid, diploid, and tetraploid HAP1 cell lines, along with diploid and tetraploid RPE1 cell lines. The analysis showed that both the complexity of karyotype formation and the level of aneuploidy significantly increase with ploidy. Additionally, karyotype refinement occurs across different ploidy states and cell lines, showing a degree of aneuploidy pattern specificity and uniformity. Notably, the reversine adaptation of tetraploid HAP1 led to the selection of double losses of chromosome 13q. To investigate the impact of double versus single losses on the adaptation of tetraploid cells, I deleted one or two copies of chromosome arms 13q and 6p in non-adapted tetraploid HAP1. This process proved more complex due to the emergence of additional nonspecific aneuploidies alongside the intended deletions. Nonetheless, four engineered tetraploid HAP1 cell lines (two with deletions of chr. 13q and two with deletions of chr. 6p) successfully demonstrated reversine resistance, emphasizing the critical roles of CDC16 and p31commet from these chromosomal regions. This study sheds light on how ploidy influences aneuploidy dynamics and provides insights into the adaptation mechanisms of tetraploid cancer cells.

Zusammenfassung

Abnormale Chromosomenzahlen oder Aneuploidien sind in mehr als 90 % der soliden Tumoren vorhanden, wobei über 30 % dieser Krebszellen polyploid sind. Aneuploidie ist normalerweise schädlich, kann jedoch bestimmte Fitnessvorteile in Krebszellen bieten. Höhere Raten von Chromosomenfehlverteilung führen zu chromosomaler Instabilität (CIN), die verschiedene Karyotyp-Komplexitäten bietet, die unter bestimmten Stressbedingungen von Vorteil sein können. Polyploide Krebszellen weisen höhere Raten von CIN auf, was zu einer größeren genetischen Heterogenität im Vergleich zu diploiden Zellen führt. Adell und Klockner (2023) verfolgten die Entwicklung komplexer Karyotypen in diploiden Zelllinien, die an den Inhibitor des Spindel-Assembly-Checkpoint, Reversin, angepasst wurden, und identifizierten, dass der selektive Verlust der Chromosomen 13q und 6p zu Reversin-Resistenz führt, bedingt durch die Gene CDC16 und p31commet, die sich auf diesen Chromosomen befinden (Adell et al., 2023). Parallel dazu führte A. Adell dasselbe Anpassungsprotokoll an menschlichen Zelllinien aus haploiden und tetraploiden Hintergründen durch. In diesem Bericht untersuchte ich Aneuploidiemuster in haploiden, diploiden und tetraploiden HAP1-Zelllinien sowie in diploiden und tetraploiden RPE1-Zelllinien. Die Analyse zeigte, dass sowohl die Komplexität der Karyotypbildung als auch der Grad der Aneuploidie signifikant mit der Ploidie ansteigen. Darüber hinaus findet eine Verfeinerung des Karyotyps über verschiedene Ploidystufen und Zelllinien hinweg statt, was einen Grad an Spezifität und Einheitlichkeit der Aneuploidiemuster zeigt. Bemerkenswert ist, dass die Reversin-Anpassung der tetraploiden HAP1-Zellen zur Selektion doppelter Verluste des Chromosoms 13q führte. Um den Einfluss von doppelten gegenüber einzelnen Verlusten auf die Anpassung tetraploider Zellen zu untersuchen, löschte ich eine oder zwei Kopien der Chromosomenarme 13q und 6p in nicht angepassten tetraploiden HAP1-Zellen. Dieser Prozess erwies sich als komplexer, da zusätzliche unspezifische Aneuploidien neben den beabsichtigten Deletionen auftraten. Dennoch zeigten vier konstruierte tetraploide HAP1-Zelllinien (zwei mit Deletionen von chr. 13q und zwei mit Deletionen von chr. 6p) erfolgreich Reversin-Resistenz und betonten damit die entscheidenden Rollen von CDC16 und p31commet aus diesen chromosomalen Regionen. Diese Studie

beleuchtet, wie Ploidie die Dynamik der Aneuploidie beeinflusst und gibt Einblicke in die Anpassungsmechanismen von tetraploiden Krebszellen.